13 Dynamical Mean-Field and Dynamical Cluster Approximation Based Theory of Superconductivity

Thomas A. Maier
Oak Ridge National Laboratory
Oak Ridge, Tennessee

Contents

E. Pavarini, E. Koch, A. Lichtenstein, and D. Vollhardt (eds.)
DMFT: From Infinite Dimensions to Real Materials
Modeling and Simulation Vol. 8
Forschungszentrum Jülich, 2018, ISBN 978-3-95806-313-6
http://www.cond-mat.de/events/correl18

1 Introduction

The collective behavior of electrons in solids gives rise to a range of different emergent phenomena, including magnetism, the fractional quantum Hall effect, and superconductivity. Of these, superconductivity is perhaps the most fascinating state that has captivated generations of physicists over more than a century. When cooled below a critical temperature T_c, superconductors exhibit conductance without resistance, the property that underlies most applications of superconductors, including power transmission and generation as well as medical applications. A second and equally important effect observed in superconductors is the complete expulsion of an external magnetic field during its transition to the superconducting state (the Meissner-Ochsenfeld effect). This repulsion of magnetic fields can be stronger than gravity which leads to levitation, the most fascinating manifestation of superconductivity. Fundamentally, it implies that the electrons in superconductors behave collectively.

Conceptually, two main ingredients, illustrated in Fig. 1, are necessary to understand the superconducting state [1]: (1) Electrons form boson-like Cooper pairs driven by a net attractive interaction; (2) These Cooper pairs condense into a coherent macroscopic quantum state analogous to a Bose-Einstein condensate. The energy required to break up the pairs (also called energy gap) suppresses the scattering processes from defects and impurities that would otherwise give rise to electrical resistance in normal conductors.

But why would two negatively charged electrons, which repel each other because of the Coulomb repulsion, would be attracted to form pairs? For conventional superconductors, which include many elemental metals such as Hg, Al, and Nb, the attractive force that binds the electrons arises from the interaction between the negatively charged electrons and the positively charged ions. The distortion of the ion lattice left behind by the motion of an electron attracts a second electron and thus results in an effective attractive interaction between the electrons. This attraction is local in space, resulting in an s-wave structure of the Cooper pair wave-function and thus an isotropic s-wave gap in momentum space. But since the ion dynamics is slow compared

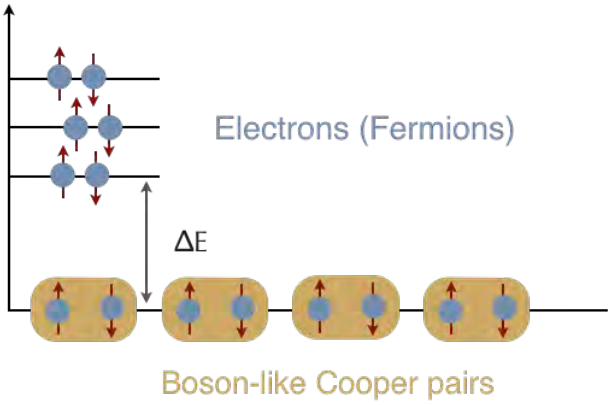

Fig. 1: Main conceptual ingredients of the BCS theory of superconductivity: *(1) Through a net attractive interaction, electrons form Cooper pairs and (2) the Cooper pairs become phase coherent and condense into a single macroscopic quantum state. The binding energy ΔE required to break up a pair suppresses the scattering processes that lead to resistance.*

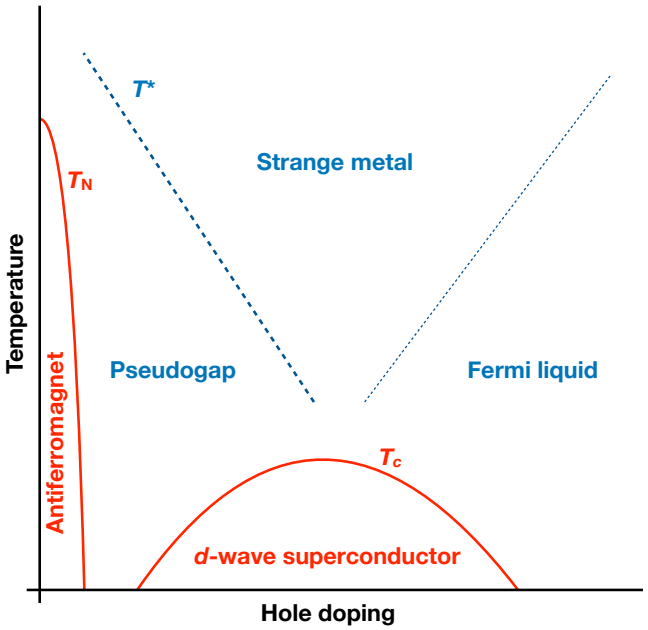

Fig. 2: Schematic temperature-doping phase diagram of the cuprate high-temperature superconductors: *The d-wave superconducting state below the critical temperature T_c emerges upon hole doping of the antiferromagnetic parent compound. Upon cooling, it arises from a normal state that hosts a pseudogap at low doping, where an energy gap is present in the electronic excitations, or a strange metal non-Fermi liquid phase at higher doping. BCS theory is not adequate to describe this situation and non-perturbative approaches are necessary to accurately treat the electron-electron correlations that give rise to these phases.*

to the electrons, it is strongly retarded in time, i.e., active at long time scales, where the effectively instantaneous Coulomb repulsion can be overcome. These concepts are well described and understood within a rigorous theoretical foundation, the BCS (Bardeen-Cooper-Schrieffer) theory [2, 1], and its extension, the Migdal-Eliashberg theory [3, 4].

Superconductivity in heavy fermion materials, copper-oxygen, and iron-based materials and other related compounds, however, is thought to arise from a different mechanism than the electron-phonon mechanism [5]. While the two main conceptual ingredients of BCS theory, i.e., the formation of Cooper pairs and their condensation into a macroscopic quantum state, still hold, the pairing mechanism that leads to the attraction of electrons is believed to be different from the electron-phonon mechanism. Because of the strong local Coulomb repulsion in these systems, local s-wave pairing is energetically unfavorable and the Cooper pair wave function is found to have a different symmetry; in the cuprates, for example, the pairs are bound in a $d_{x^2-y^2}$-wave state, in which the pair wave function changes sign in momentum space and which corresponds to pair formation on nearest-neighbor atom positions in the crystal lattice. Similarly, in the iron-based superconductors, the pairs are believed to form an extended, sign changing s-wave state, in which the local amplitude is strongly reduced. As we will see, such a pair structure with a sign change indicates that the pairing interaction is actually repulsive in momentum space, in marked contrast to the conventional electron-phonon case. It is therefore generally accepted that pairing in these "unconventional" superconductors has a different

origin, and most likely arises from the strong magnetic interactions or fluctuations between the electron spins that result in an antiferromagnetic phase in the undoped parent compounds. Moreover, BCS theory assumes that the superconducting state is created from a normal metallic Fermi liquid state with well defined quasiparticles. In contrast, the normal state in many unconventional superconductors is everything but normal (see Fig. 2). Strong electron-electron correlations in these systems often lead to non-Fermi liquid behavior and BCS theory is not adequate. One instead needs a non-perturbative approach that can handle the strong correlations and which does not assume a Fermi liquid normal state as a starting point. Dynamical mean-field theory (DMFT) [6] and the dynamical cluster approximation (DCA) [7] provide such a tool, which allows us to study how superconductivity emerges in systems where the normal state behavior is governed by strong electron correlations.

These lecture notes are concerned with such unconventional systems, in which superconductivity arises from the strong local Coulomb repulsion between the electrons. Given that superconductivity requires electrons to form pairs, this seems like a paradox. The goal of this lecture is to demonstrate how DMFT and DCA calculations have helped us resolve this paradox. Following a pedagogical discussion of the DMFT and DCA frameworks to study superconductivity, we highlight a set of applications that showcase the ability of these approaches to provide important insight. In this lecture we assume a basic familiarity with BCS, DMFT, and DCA theory.

2 Dynamical mean-field theory and dynamical cluster approximation

2.1 Preliminary remarks

To keep things simple, we will focus most of these lecture notes on one of the simplest models of correlated electron systems, the single-band Hubbard model [8]. Its Hamiltonian

$$H = \sum_{ij,\sigma} t_{ij}\, c^\dagger_{i\sigma} c_{j\sigma} + U \sum_i n_{i\uparrow} n_{i\downarrow} \tag{1}$$

is divided into a non-interacting part H_0 given by the first term and an interacting part $H_{\rm int}$ given by the second term. Here $c^{(\dagger)}_{i\sigma}$ destroys (creates) an electron on site i with spin σ and $n_{i\sigma} = c^\dagger_{i\sigma} c_{i\sigma}$ is the corresponding number operator. The first (H_0) term describes the hopping of electrons between sites i and j with amplitude t_{ij}, and the second ($H_{\rm int}$) term raises the energy by the Coulomb repulsion U when two electrons with opposite spin reside on the same site. If not otherwise noted, we consider the sites in this model to form a two-dimensional (2D) square lattice with a hopping $t_{ij} = -t$ if i and j are nearest-neighbor sites. Despite its simplicity, this model is commonly believed to provide a description of the generic physics of the cuprate high-temperature superconductors [9], in which photoemission experiments find a single electronic band crossing the Fermi level.

The single-particle dynamics of the Hubbard Hamiltonian at finite temperatures is described by the thermodynamic Green function and its Fourier-transform to Matsubara frequencies and

momentum space

$$G_{ij,\sigma} = -\left\langle T_\tau c_{i\sigma}(\tau) c^\dagger_{j\sigma} \right\rangle \tag{2}$$

$$G_{ij,\sigma}(i\omega_n) = \int_0^\beta d\tau\, e^{i\omega_n \tau}\, G_{ij,\sigma}(\tau)\,, \quad \omega_n = (2n+1)\pi T \tag{3}$$

$$G_\sigma(\boldsymbol{k}, i\omega_n) \equiv \langle\langle c_{\boldsymbol{k}\sigma}; c^\dagger_{\boldsymbol{k}\sigma}\rangle\rangle_{i\omega_n} = \frac{1}{N}\sum_{ij} e^{i\boldsymbol{k}(\boldsymbol{r}_i - \boldsymbol{r}_j)}\, G_{ij,\sigma}(i\omega_n)\,. \tag{4}$$

Here τ is the imaginary time, T_τ the time ordering operator, $\beta = 1/T$ the inverse temperature and $\omega_n = (2n+1)\pi T$ are the fermionic Matsubara frequencies. For problems with translational symmetry in space and time, the Green function becomes diagonal in momentum $\boldsymbol{k}$ and frequency $i\omega_n$ as stated in Eqs. (3) and (4). The Green function G_0 of the non-interacting system, i.e. $H = H_0$, is given by

$$G_0(\boldsymbol{k}, i\omega_n) = \frac{1}{i\omega_n + \mu - \varepsilon_{\boldsymbol{k}}}\,, \tag{5}$$

where μ is the chemical potential and $\varepsilon_{\boldsymbol{k}}$ the dispersion, obtained from a Fourier-transform of the hopping t_{ij}. For our 2D model with only nearest neighbor hopping t, we have

$$\varepsilon_{\boldsymbol{k}} = -2t(\cos k_x + \cos k_y) \tag{6}$$

with $\boldsymbol{k} = (k_x, k_y)$. Finally, the Dyson equation

$$G(\boldsymbol{k}, i\omega_n) = \frac{1}{G_0^{-1}(\boldsymbol{k}, i\omega_n) - \Sigma(\boldsymbol{k}, i\omega_n)}\,. \tag{7}$$

defines the self-energy $\Sigma(\boldsymbol{k}, i\omega_n)$ as the difference between the (inverse) non-interacting Green function G_0 and the fully renormalized Green function G and thus describes the effects of the interaction term H_{int} on the single-particle dynamics.

2.2 General framework for the normal state

Calculating the Green function G and self-energy Σ in the thermodynamic limit is prohibitively expensive as the problem size grows exponentially in the number of degrees of freedom (sites in the Hubbard model). The DMFT and DCA approaches reduce this complexity by representing the infinite-size system by a reduced-size cluster, and use coarse-graining in momentum space to retain information about the degrees of freedom (sites) not contained on the cluster [7]. In DMFT the cluster consists only of a single site, called the impurity site, while in DCA the cluster has several sites. The size of the cluster is controlled by the way the momentum space is coarse-grained. Fig. 3 shows several examples starting from the single-site ($N_c = 1$) DMFT impurity. The DCA is obtained for $N_c > 1$. It reduces to the DMFT for $N_c = 1$ and approaches the exact result for $N_c \to \infty$. Because the DCA includes the DMFT as a limiting case, we restrict the following discussion to the DCA.

The first Brillouin zone is split into N_c patches of equal size. As illustrated in Fig. 3, each patch is represented by a cluster momentum $\boldsymbol{K}$ at its center. The basic assumption of the

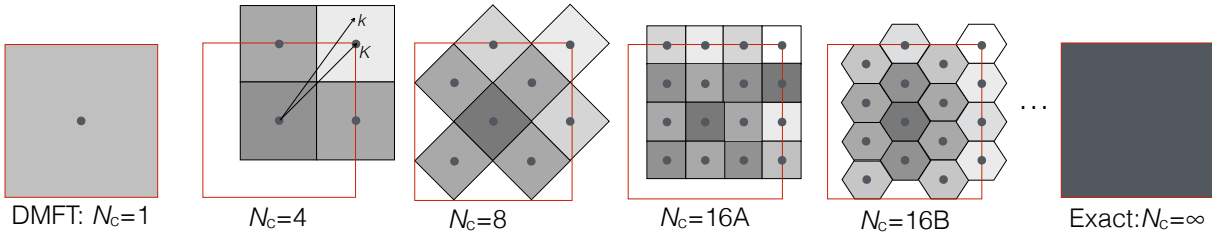

Fig. 3: Coarse-graining of momentum space: *At the heart of the DCA (and DMFT) methods is a partitioning of the first Brillouin zone into N_c patches over which the Green function is coarse-grained (averaged) to represent the system by a reduced number of N_c "cluster" degrees of freedom. The bulk degrees of freedom not included on the cluster are taken into account as a mean-field. For $N_c = 1$, the dynamical mean-field approximation is recovered, while for $N_c \to \infty$, one obtains the exact result. For a given cluster size N_c, one can have different locations and shapes of the coarse-graining patches, as illustrated for N_c =16A and 16B.*

approximation is that the self-energy is only weakly momentum dependent (or purely local in DMFT), so that its momentum dependence is well represented by the coarse-grid of cluster momenta $\boldsymbol{K}$, i.e.,

$$\Sigma(\boldsymbol{k}, i\omega_n) \simeq \Sigma_c(\boldsymbol{K}, i\omega_n) \text{ (in DCA) or } \Sigma(\boldsymbol{k}, i\omega_n) \simeq \Sigma_{ii}(i\omega_n) \text{ (in DMFT)}. \tag{8}$$

Here, $\Sigma_c(\boldsymbol{K}, i\omega_n)$ is the self-energy of a cluster of size N_c, and $\Sigma_{ii}(i\omega_n)$ that of a single-site impurity in DMFT. One then sets up an effective cluster problem to calculate $\Sigma_c(\boldsymbol{K}, i\omega_n)$ or $\Sigma_{ii}(i\omega_n)$. To this end, the Green function is coarse-grained over the DCA patches (or the full Brillouin zone in DMFT)

$$\bar{G}(\boldsymbol{K}, i\omega_n) = \frac{N_c}{N} \sum_{\boldsymbol{k}\in\mathcal{P}_{\boldsymbol{K}}} G(\boldsymbol{k}, i\omega_n) = \frac{N_c}{N} \sum_{\boldsymbol{k}\in\mathcal{P}_{\boldsymbol{K}}} \frac{1}{i\omega_n - \varepsilon_{\boldsymbol{k}} + \mu - \Sigma_c(\boldsymbol{K}, i\omega_n)}, \tag{9}$$

where $\mathcal{P}_{\boldsymbol{K}}$ is the patch centered at $\boldsymbol{K}$ containing N/N_c momenta $\boldsymbol{k}$. Note that in DMFT, the sum runs over the full Brillouin zone and the coarse-grained Green function reduces to the local Green function. Given $\bar{G}$ and Σ_c, one can then set up an algorithm, such as, for example, the quantum Monte Carlo (QMC) algorithms discussed in Refs. [10, 11], to calculate the cluster Green function. The non-interacting part of the cluster problem is defined by the cluster-excluded Green function

$$\mathcal{G}(\boldsymbol{K}, i\omega_n) = \left(\bar{G}^{-1}(\boldsymbol{K}, i\omega_n) + \Sigma_c(\boldsymbol{K}, i\omega_n)\right)^{-1}, \tag{10}$$

where the cluster self-energy has been added to avoid double counting. While $\mathcal{G}(\boldsymbol{K}, i\omega_n)$ is the Green function of a cluster of size N_c, note that the remaining lattice degrees of freedom are encoded in $\mathcal{G}$ through the use of the coarse-grained Green function $\bar{G}$. Together with the interacting part of the Hamiltonian, one then sets up the action for the effective cluster problem, which reads after Fourier-transform to real space

$$S[\phi^*, \phi] = -\int_0^\beta d\tau \int_0^\beta d\tau' \sum_{ij,\sigma} \phi^*_{i\sigma}(\tau)\, \mathcal{G}_{0,ij,\sigma}(\tau - \tau')\, \phi_{j\sigma}(\tau) + \int_0^\beta d\tau \sum_i U \phi^*_{i\uparrow}(\tau)\phi_{i\uparrow}\phi^*_{i\downarrow}(\tau)\phi_{i\downarrow}(\tau)\,. \tag{11}$$

Here ϕ and ϕ^* are the Grassmann variables corresponding to the operators c and $c^\dagger$, respectively. From this the cluster Green function

$$G_{c,ij,\sigma}(\tau-\tau') = \frac{1}{Z}\int \mathcal{D}[\phi^*\phi]\,\phi_{i\sigma}(\tau)\phi^*_{j\sigma}(\tau')\,e^{-S[\phi^*,\phi]}\,, \tag{12}$$

with

$$Z = \int \mathcal{D}[\phi^*\phi]\,e^{-S[\phi^*,\phi]} \tag{13}$$

the partition function, is evaluated and used to determine the cluster self-energy

$$\Sigma_c(\boldsymbol{K}, i\omega_n) = \mathcal{G}_0^{-1}(\boldsymbol{K}, i\omega_n) - G_c^{-1}(\boldsymbol{K}, i\omega_n)\,. \tag{14}$$

Then, using this new result for $\Sigma_c(\boldsymbol{K}, i\omega_n)$ in Eq. (9), these steps are iterated to convergence. We note that this DCA algorithm was recently extended into the DCA$^+$ method [12] through the inclusion of a self-energy $\Sigma(\boldsymbol{k}, i\omega_n)$ with continuous momentum $\boldsymbol{k}$ dependence that replaces the piecewise constant self-energy $\Sigma_c(\boldsymbol{K}, i\omega_n)$ in the coarse-graining step, while leaving the cluster problem unchanged. This has the benefit that results depend less on the shape of the cluster that is being used.

2.3 Nambu-Gorkov formalism

In this section we generalize the DCA (and DMFT) formalism to perform calculations in the symmetry broken superconducting state. This phase is signaled by an order parameter that describes the finite expectation value for the creation of a pair of electrons in time-reversed momentum states

$$\Delta_{\boldsymbol{k}} = \langle c_{\boldsymbol{k}\uparrow} c_{-\boldsymbol{k}\downarrow}\rangle \neq 0 \text{ for some } \boldsymbol{k}\,. \tag{15}$$

Here we restrict the discussion to spin singlet pairs and note that $\Delta_{\boldsymbol{k}}$ can only be finite for a grand canonical ensemble in which the particle number is not fixed. This is not a problem for DMFT or DCA, since these approaches are formulated for the grand canonical ensemble. The momentum structure of $\Delta_{\boldsymbol{k}}$ determines the symmetry of the superconducting state. Examples are $\Delta_{\boldsymbol{k}} \propto 1$ (s-wave), $\cos k_x + \cos k_y$ (extended s-wave), $\cos k_x - \cos k_y$ ($d_{x^2-y^2}$-wave), $\sin k_x \sin k_y$ (d_{xy}-wave) or $a \sin k_x + b \sin k_y$ (p-wave). Because $\Delta_{\boldsymbol{k}}$ is finite in the superconducting phase, one has, in addition to the normal Green function

$$G(\boldsymbol{k}, i\omega_n) = \langle\langle c_{\boldsymbol{k}\uparrow}; c^\dagger_{\boldsymbol{k}\uparrow}\rangle\rangle_{i\omega_n} \tag{16}$$

a finite anomalous Green function

$$F(\boldsymbol{k}, i\omega_n) = \langle\langle c_{\boldsymbol{k}\uparrow}; c_{-\boldsymbol{k}\downarrow}\rangle\rangle_{i\omega_n}\,. \tag{17}$$

Using the concept of Nambu spinors [1]

$$\Psi^\dagger_{\boldsymbol{k}} = \left(c^\dagger_{\boldsymbol{k}\uparrow},\, c_{-\boldsymbol{k}\downarrow}\right)\,,\; \Psi_{\boldsymbol{k}} = \begin{pmatrix} c_{\boldsymbol{k}\uparrow} \\ c^\dagger_{-\boldsymbol{k}\downarrow}\end{pmatrix} \tag{18}$$

one then defines the Green function matrix in Nambu space [1]

$$\mathbf{G}(\boldsymbol{k}, i\omega_n) = \langle\langle \Psi_{\boldsymbol{k}}; \Psi_{\boldsymbol{k}}^\dagger \rangle\rangle_{i\omega_n} = \begin{pmatrix} G\left(\boldsymbol{k}, i\omega_n\right) & F\left(\boldsymbol{k}, i\omega_n\right) \\ F^*(\boldsymbol{k}, -i\omega_n) & -G^*(\boldsymbol{k}, i\omega_n) \end{pmatrix}, \tag{19}$$

which contains information about both the normal and the anomalous Green function. Note that the $\mathbf{G}$ matrix contains only two independent matrix elements G and F. The elements in the second row are related to those in the first row by general symmetry relations for Green functions. In the presence of an external pairing field $\eta(\boldsymbol{k}) = \eta'(\boldsymbol{k}) + i\eta''(\boldsymbol{k})$, which couples to $c_{-\boldsymbol{k}\downarrow} c_{\boldsymbol{k}\uparrow}$, the non-interacting part of the Hubbard Hamiltonian becomes

$$H_0 = \sum_{\boldsymbol{k}} \Psi_{\boldsymbol{k}}^\dagger \Big(\epsilon_{\boldsymbol{k}} \sigma_3 - \eta'(\boldsymbol{k}) \sigma_1 + \eta''(\boldsymbol{k}) \sigma_2 \Big) \Psi_{\boldsymbol{k}} \,, \tag{20}$$

where the σ_i are the Pauli spin matrices

$$\sigma_0 = \begin{pmatrix} 1 & 0 \\ 0 & 1 \end{pmatrix}, \, \sigma_1 = \begin{pmatrix} 0 & 1 \\ 1 & 0 \end{pmatrix}, \, \sigma_2 = \begin{pmatrix} 0 & -i \\ i & 0 \end{pmatrix}, \, \sigma_3 = \begin{pmatrix} 1 & 0 \\ 0 & -1 \end{pmatrix}. \tag{21}$$

With this, the lattice Green function in the superconducting state becomes

$$\mathbf{G}(\boldsymbol{k}, i\omega_n) = \Big(i\omega_n \sigma_0 - (\varepsilon_{\boldsymbol{k}} - \mu)\sigma_3 - \eta'(\boldsymbol{k})\sigma_1 - \eta''(\boldsymbol{k})\sigma_2 - \mathbf{\Sigma}_c(\boldsymbol{K}, i\omega_n) \Big)^{-1} \tag{22}$$

with the cluster self-energy matrix

$$\mathbf{\Sigma}_c(\boldsymbol{K}, i\omega_n) = \begin{pmatrix} \Sigma_c\left(\boldsymbol{K}, i\omega_n\right) & \phi_c\left(\boldsymbol{K}, i\omega_n\right) \\ \phi_c^*(\boldsymbol{K}, -i\omega_n) & -\Sigma_c^*(\boldsymbol{K}, i\omega_n) \end{pmatrix}. \tag{23}$$

Here, the diagonal parts $\Sigma_c(\boldsymbol{K}, i\omega_n)$ describe the usual quasiparticle renormalization, while the off-diagonal parts $\phi_c(\boldsymbol{K}, i\omega_n)$ contain information about the momentum and frequency dependence of the pairing state. As in the normal state, the coarse-grained Green function

$$\bar{\mathbf{G}}(\boldsymbol{K}, i\omega_n) = \frac{N_c}{N} \sum_{\boldsymbol{k} \in \mathcal{P}_{\boldsymbol{K}}} \mathbf{G}(\boldsymbol{k}, i\omega_n) = \begin{pmatrix} \bar{G}\left(\boldsymbol{K}, i\omega_n\right) & \bar{F}\left(\boldsymbol{K}, i\omega_n\right) \\ \bar{F}^*(\boldsymbol{K}, -i\omega_n) & -\bar{G}^*(\boldsymbol{K}, i\omega_n) \end{pmatrix} \tag{24}$$

is then used to calculate the corresponding non-interacting (cluster-excluded) Green function matrix

$$\mathcal{G}_0(\boldsymbol{K}, i\omega_n) = \big(\bar{\mathbf{G}}^{-1}(\boldsymbol{K}, i\omega_n) + \mathbf{\Sigma}_c(\boldsymbol{K}, i\omega_n) \big)^{-1}. \tag{25}$$

To calculate $\mathbf{\Sigma}_c(\boldsymbol{K}, i\omega_n)$, an effective cluster model is set up using $\mathcal{G}_0$ together with the interaction U

$$\begin{aligned} S[\boldsymbol{\Psi}^*, \boldsymbol{\Psi}] = &- \int_0^\beta d\tau \int_0^\beta d\tau' \sum_{ij} \boldsymbol{\Psi}_i^\dagger(\tau) \, \mathcal{G}_{0,ij}(\tau - \tau') \, \boldsymbol{\Psi}_j(\tau') \\ &+ \frac{U}{2} \int_0^\beta d\tau \sum_i [\boldsymbol{\Psi}_i^\dagger(\tau) \sigma_3 \boldsymbol{\Psi}_i(\tau)][\boldsymbol{\Psi}_i^\dagger(\tau) \sigma_3 \boldsymbol{\Psi}_i(\tau)] \,, \end{aligned} \tag{26}$$

where the $\boldsymbol{\Psi}_i^\dagger$ and $\boldsymbol{\Psi}_i$ are spinors $\boldsymbol{\Psi}_i^\dagger = (\phi_{i\uparrow}^*, \phi_{i\downarrow})$ of Grassmann variables $\phi_{i\sigma}^\dagger$ and $\phi_{i\sigma}$ which generate coherent states corresponding to the fermionic operators $c_{i\sigma}^\dagger$ and $c_{i\sigma}$, respectively. From this, the cluster Green function

$$\mathbf{G}_{c,ij}(\tau - \tau') = \frac{1}{Z}\int \mathcal{D}[\boldsymbol{\Psi}^*\boldsymbol{\Psi}]\, \boldsymbol{\Psi}_i(\tau)\boldsymbol{\Psi}_j(\tau')\, e^{-S[\boldsymbol{\Psi}^*,\boldsymbol{\Psi}]} \tag{27}$$

where

$$Z = \int \mathcal{D}[\boldsymbol{\Psi}^*\boldsymbol{\Psi}]\, e^{-S[\boldsymbol{\Psi}^*,\boldsymbol{\Psi}]} \tag{28}$$

is the partition function, is calculated using a cluster solver algorithm, such as e.g., a QMC algorithm [13] or a non-crossing approximation (NCA) [14], and used to determine the cluster self-energy

$$\boldsymbol{\Sigma}_c(\boldsymbol{K}, i\omega_n) = \mathcal{G}_0^{-1}(\boldsymbol{K}, i\omega_n) - \mathbf{G}_c^{-1}(\boldsymbol{K}, i\omega_n)\,. \tag{29}$$

Then, just as in the normal state, using this new result for $\boldsymbol{\Sigma}_c(\boldsymbol{K}, i\omega_n)$ in Eq. (22), steps (22) to (29) are iterated to self-consistency. After convergence, the superconducting order parameter

$$\bar{\Delta}(\boldsymbol{K}) = \frac{N_c}{N}\sum_{\boldsymbol{k}\in\mathcal{P}_{\boldsymbol{K}}} \langle c_{\boldsymbol{k}\uparrow} c_{-\boldsymbol{k}\downarrow}\rangle = \bar{F}(\boldsymbol{K}, \tau = 0) \tag{30}$$

is calculated from the coarse-grained anomalous Green function $\bar{F}$.
Two notes are in order:

- Usually one is interested in an instability to a superconducting phase in the absence of an external pair-field, i.e., spontaneous $U(1)$ gauge symmetry breaking. In this case, the calculation is initialized with a finite pair-field $\eta(\boldsymbol{k})$ with a given momentum structure. After the first few iterations, the pair-field is switched off, and the system relaxes. If the calculation converges to a finite order parameter $\bar{\Delta}(\boldsymbol{K})$, the system is in the superconducting phase, otherwise it is in the normal state.

- The symmetry of the superconducting order is given by the momentum structure of the coarse-grained $\bar{\Delta}(\boldsymbol{K})$ and therefore restricted by the cluster size and geometry. In the case of the DMFT, when $N_c = 1$, $\bar{\Delta}(\boldsymbol{K}) = \bar{\Delta}$ is local, and therefore only superconducting states with a local contribution such as s-wave or extended s-wave can be described. Larger clusters are necessary to describe order parameters with a symmetry less than the lattice symmetry. For example, a 2×2 cluster is the smallest cluster to describe phases with a $d_{x^2-y^2}$-wave symmetry which transforms according to $\cos k_x - \cos k_y$.

As a typical example of such a calculation, Fig. 4 shows DCA results from Ref. [14] for the superconducting state of a 2D Hubbard model with $U = 12t$ and electron filling $\langle n\rangle = 0.81$ for a temperature $T = 0.05t$. These results were obtained with a non-crossing approximation to solve the DCA effective cluster problem on an $N_c = 4$ site 2×2 cluster [15]. One sees that the anomalous Green function $\bar{F}(\boldsymbol{K}, \omega) \equiv \bar{G}_{12}(\boldsymbol{K}, i\omega_n)$ is finite, switches sign between $\boldsymbol{K} = (\pi, 0)$ and $(0, \pi)$, and vanishes for $\boldsymbol{K} = 0$ and (π, π). This is exactly what one expects for

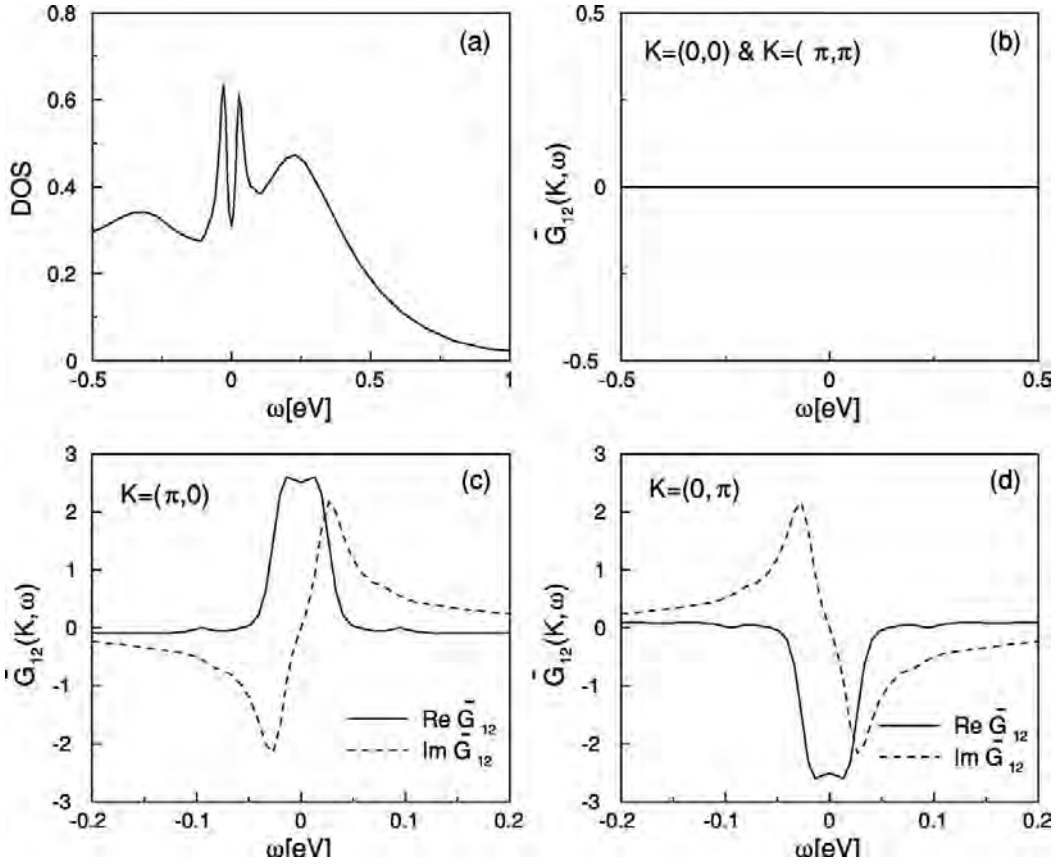

Fig. 4: *d*-wave superconducting state in a 2D Hubbard model: *DCA/NCA calculation for an $N_c = 4$ site 2×2 cluster. Density of states near the chemical potential (a), and coarse-grained anomalous Green function $\bar{G}_{12}(\boldsymbol{K}, i\omega_n \to \omega + i\delta) \equiv \bar{F}(\boldsymbol{K}, \omega + i\delta)$ (b), (c), and (d) for a system with electron filling $\langle n \rangle = 0.81$, temperature $T = 0.05t$ and Coulomb repulsion $U = 12t$ for the different cluster momenta $\boldsymbol{K}$. Figure from [14].*

a $d_{x^2-y^2}$-wave order parameter that transforms according to $\Delta(\boldsymbol{k}) \propto \cos k_x - \cos k_y$. Since the DCA patches about $\boldsymbol{K} = 0$ and (π, π) contain equal parts of positive and negative contributions of $\Delta(\boldsymbol{k})$, the coarse-grained result averaged over these patches vanishes, while $\Delta(\boldsymbol{k})$ has the same sign over each of the patches centered at $(\pi, 0)$ and $(0, \pi)$ and switches sign between them. The superconducting gap that arises from the finite pair amplitude is reflected in the density of states (DOS) shown in the upper left panel, where the lower Hubbard subband of the full spectrum is shown.

2.4 Pair-field susceptibility

An alternative way to identify an instability towards a superconducting phase (or any symmetry broken phase for that matter) is to calculate the response of the system to an applied field (pair-field in the case of superconductivity), i.e., the susceptibility, and then extrapolate that response to the limit of a vanishing field. Spontaneous symmetry breaking occurs when the susceptibility diverges in that limit.

General formalism

In linear response theory, the superconducting response to an external pair-field η_α, where α specifies the symmetry (s-wave, d-wave, etc.), is given by the pair-field susceptibility

$$P_\alpha(T) = \int_0^\beta d\tau \, \langle \Delta_\alpha(\tau) \Delta_\alpha^\dagger(0) \rangle \tag{31}$$

since the pair-field η_α couples to the pairing operator

$$\Delta_\alpha^\dagger = \frac{1}{\sqrt{N}} \sum_{\boldsymbol{k}} g_\alpha(\boldsymbol{k}) \, c_{\boldsymbol{k}\uparrow}^\dagger c_{-\boldsymbol{k}\downarrow}^\dagger \,, \tag{32}$$

and we are interested in the response Δ_α of the system to the pair-field. Here $g_\alpha(k)$ is the form-factor corresponding to the symmetry of interest, i.e., $g_d(\boldsymbol{k}) = \cos k_x - \cos k_y$ for a $d_{x^2-y^2}$ state, for example. Instead of calculating the correlation function in Eq. (31) directly, the pair-field susceptibility may be calculated within the formalism described in then previous section 2.3. This is done by keeping the external pair-field η_α finite throughout the calculation and measuring the order parameter Δ_α at convergence. If this is done for a number of different magnitudes of the external field η_α, one has information on the η_α dependence of the order parameter $\Delta_\alpha(\eta_\alpha)$. The pair-field susceptibility P_α may then be extracted from the limit of vanishing pair-field as $P_\alpha = \left. \frac{d\Delta_\alpha(\eta_\alpha)}{d\eta_\alpha} \right|_{\eta_\alpha \to 0}$.
Alternatively, one may calculate the correlation function in Eq. (31) directly in the normal state of the system. This does not require the Nambu-Gorkov formalism discussed in Sec. 2.3, i.e., the calculation may be carried out in the normal state. What is required, however, is a calculation of the 4-point two-particle Green function [10]

$$G_{2,\sigma_1 \ldots \sigma_4}(x_1, x_2; x_3, x_4) = -\langle T_\tau c_{\sigma_1}(x_1) c_{\sigma_2}(x_2) c_{\sigma_3}^\dagger(x_3) c_{\sigma_4}^\dagger(x_4) \rangle \,, \tag{33}$$

where the combined index $x_i = (\boldsymbol{X}_i, \tau_i)$ has both spatial $\boldsymbol{X}_i$ and imaginary time τ_i coordinates. Fourier-transforming on both the space and time variables gives $G_{2\sigma_1 \ldots \sigma_4}(k_4, k_3; k_2, k_1)$ with $k = (\boldsymbol{k}, i\omega_n)$. From this, one may then calculate the pair-field susceptibility as

$$P_\alpha(T) = \frac{T^2}{N^2} \sum_{k,k'} g_\alpha(\boldsymbol{k}) \, G_{2,\uparrow\downarrow\downarrow\uparrow}(k, -k, -k', k') \, g_\alpha(\boldsymbol{k}'). \tag{34}$$

The way G_2 is calculated in the DCA algorithm is similar to the way G is calculated at the single-particle level. Just as the Dyson equation (7) relates the Green function to the self-energy, the Bethe-Salpeter equation (BSE) relates G_2 to the irreducible particle-particle vertex function $\Gamma^{\mathrm{pp}}(k, -k; -k', k')$. It reads

$$\begin{aligned} G_{2,\uparrow\downarrow\downarrow\uparrow}(k, -k, -k', k') = G_\uparrow(k) \, G_\downarrow(-k) \delta_{k,k'} + \frac{T}{N} \sum_{k''} G_\uparrow(k) \, G_\downarrow(-k) \\ \times \Gamma^{\mathrm{pp}}(k, -k, -k'', k'') \, G_{2,\uparrow\downarrow\downarrow\uparrow}(k'', -k'', -k', k') \end{aligned} \tag{35}$$

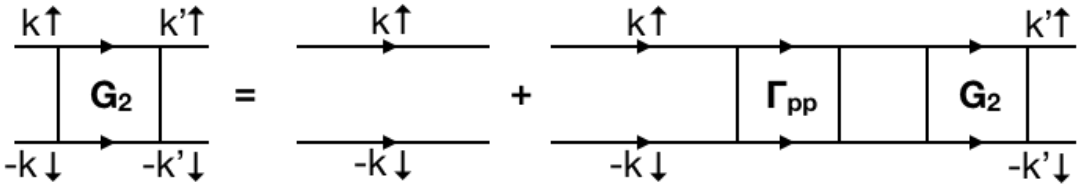

Fig. 5: Feynman diagrams for the Bethe-Salpeter equation: *The two-particle Green function G_2 in the particle-particle channel on the left hand side has a bare contribution (first diagram on the right-hand side) that describes the propagation of a pair of electrons in time-reversed momentum and spin states, and a vertex contribution (second diagram) that describes the (repeated) scattering of the pair due to the interactions in the Hamiltonian.*

and is schematically shown in Fig. 5. This equation describes the propagation of a pair of electrons in time-reversed momentum and spin states and the repeated scattering of this pair due to the Coulomb term in the Hamiltonian.

Just as the self-energy $\Sigma(\boldsymbol{k}, i\omega_n)$ is approximated by the cluster self-energy $\Sigma_c(\boldsymbol{K}, i\omega_n)$, the irreducible vertex function $\Gamma^{\rm pp}$ is approximated by the corresponding cluster irreducible vertex function [10]

$$\Gamma^{\rm pp}(k,-k,-k',k') \approx \Gamma_c^{\rm pp}(K,-K,-K',K'), \tag{36}$$

where $K = (\boldsymbol{K}, i\omega_n)$ and $K' = (\boldsymbol{K}', i\omega_{n'})$. Just as the self-energy, the cluster irreducible vertex $\Gamma_c^{\rm pp}$ is determined from the solution of the cluster problem, i.e., by calculating the cluster two-particle correlation function

$$\begin{aligned} G_{2c,\uparrow\downarrow\downarrow\uparrow}(K,-K,-K',K') = G_{c,\uparrow}(K)\, G_{c,\downarrow}(-K)\delta_{K,K'} + \frac{T}{N_c}\sum_{K''} G_{c,\uparrow}(K)\, G_{c,\downarrow}(-K) \\ \times \Gamma_{c,pp}(K,-K,-K'',K'')\, G_{2c,\uparrow\downarrow\downarrow\uparrow}(K'',-K'',-K',K')\,. \end{aligned} \tag{37}$$

Defining $[\mathbf{G}_{2c}]_{K,K'} \equiv G_{2c,\uparrow\downarrow\downarrow\uparrow}(K,-K,-K',K')$, $[\mathbf{G}^0_{2c}]_{K,K'} = G_{c,\uparrow}(K)\, G_{c,\downarrow}(-K)\, \delta_{K,K'}$ and $[\mathbf{\Gamma}_c^{\rm pp}]_{K,K'} = \frac{T}{N_c}\Gamma_c^{\rm pp}(K,-K,-K',K')$, and writing Eq. (37) in matrix notation in K, K', one then has

$$\mathbf{\Gamma}_{c,pp} = [\mathbf{G}^0_{2c}]^{-1} - [\mathbf{G}_{2c}]^{-1}\,. \tag{38}$$

Using the cluster vertex $\Gamma_c^{\rm pp}(K,-K,-K',K')$ in the BSE for the lattice G_2, one can then calculate the coarse-grained two-particle Green function for the lattice

$$\begin{aligned} \bar{G}_{2,\uparrow\downarrow\downarrow\uparrow}(K,-K,-K',K') &= \frac{N_c^2}{N^2}\sum_{\boldsymbol{k}\in\mathcal{P}_{\boldsymbol{K}}}\sum_{\boldsymbol{k}'\in\mathcal{P}_{\boldsymbol{K}'}} G_{2,\uparrow\downarrow\downarrow\uparrow}(k,-k,-k',k') \\ &= \bar{G}^0_{2,\uparrow\downarrow}(K)\delta_{K,K'} + \frac{T}{N_c}\sum_{K''}\bar{G}^0_{2,\uparrow\downarrow}(K) \\ &\quad \times \Gamma_c^{\rm pp}(K,-K,-K'',K'')\,\bar{G}_{2,\uparrow\downarrow\downarrow\uparrow}(K'',-K'',-K',K')\,. \end{aligned} \tag{39}$$

with the coarse-grained bare propagator

$$\bar{G}^0_{2,\uparrow\downarrow}(K) = \frac{N_c}{N}\sum_{\boldsymbol{k}\in\mathcal{P}_{\boldsymbol{K}}} G_\uparrow(k)\, G_\downarrow(-k)\,. \tag{40}$$

Here we used the fact the cluster vertex $\Gamma_c^{\rm pp}(K,-K,-K',K')$ only depends on the cluster momenta $\boldsymbol{K}$ and $\boldsymbol{K}'$ so that the sum over $\boldsymbol{k}''$ in Eq. (35) can be partially carried out over the patches. The coarse-grained G_2 may then be inserted into Eq. (34) to obtain

$$P_\alpha(T) = \frac{T^2}{N_c^2} \sum_{K,K'} \bar{g}_\alpha(\boldsymbol{K})\, \bar{G}_{2,\uparrow\downarrow\downarrow\uparrow}(K,-K,-K',K')\, \bar{g}_\alpha(\boldsymbol{K}')\,, \tag{41}$$

where we have separately coarse-grained the form factor $\bar{g}_\alpha(\boldsymbol{K}) = N_c/N \sum_{\boldsymbol{k}\in\mathcal{P}_{\boldsymbol{K}}} g_\alpha(\boldsymbol{k})$. Note that one can also take into account the full $\boldsymbol{k}$ dependence of $g_\alpha(\boldsymbol{k})$ by using the modified algorithm discussed in Ref. [10].

Bethe-Salpeter eigenvalues and eigenfunctions

Writing Eq. (39) in matrix form

$$\bar{\mathbf{G}}_2 = [\mathbb{1} - \bar{\mathbf{G}}^0_{2,\uparrow\downarrow}\mathbf{\Gamma}_c^{\rm pp}]^{-1}\bar{\mathbf{G}}^0_{2,\uparrow\downarrow} = \bar{\mathbf{G}}^0_{2,\uparrow\downarrow}[\mathbb{1} - \mathbf{\Gamma}_c^{\rm pp}\bar{\mathbf{G}}^0_{2,\uparrow\downarrow}]^{-1} \tag{42}$$

we see that a divergence in $\bar{\mathbf{G}}_2$ occurs when the term in brackets vanishes. Eq. (42) can be recast in terms of the left (Φ^L_α) and right eigenvectors (Φ^R_α) of the "pairing matrix" $\mathbf{\Gamma}_c^{\rm pp}\bar{\mathbf{G}}^0_{2,\uparrow\downarrow}$, where, for example, Φ^R_α is determined from [16]

$$-\frac{T}{N_c}\sum_{K'} \Gamma_{c,pp}(K,K')\, \bar{G}^0_{2,\uparrow\downarrow}(K')\, \phi^R_\alpha(K') = \lambda_\alpha \phi^R_\alpha(K). \tag{43}$$

By transforming the term in brackets in Eq. (42) onto this eigenbasis of the pairing matrix, one can write Eq. (42) as

$$G_{2,\uparrow\downarrow\downarrow\uparrow}(K,K') = \bar{G}^0_{2,\uparrow\downarrow}(K) \sum_\alpha \frac{\phi^R_\alpha(K)\phi^L_\alpha(K')}{1-\lambda_\alpha}\,. \tag{44}$$

Since the pair-field susceptibility is given by Eq. (41), we see that a superconducting instability occurs when the leading eigenvalue λ_α becomes equal to one, and the symmetry of the corresponding state is determined by the momentum and frequency structure of $\phi^R_\alpha(K)$ and $\phi^L_\alpha(K)$. This approach is in many ways more powerful than calculating the response function directly, because here, one does not have to assume a given form factor $g_\alpha(\boldsymbol{k})$ and therefore cannot "miss" the structure of the dominant correlations.

We note the similarity of Eq. (43) to the familiar BCS gap equation

$$-\frac{1}{N}\sum_{\boldsymbol{k}'} \frac{V(\boldsymbol{k},\boldsymbol{k}')\tanh\left(\frac{\beta}{2}E_{\boldsymbol{k}'}\right)\Delta(\boldsymbol{k}')}{2E_{\boldsymbol{k}'}} = \Delta(\boldsymbol{k}'), \tag{45}$$

where $V(\boldsymbol{k},\boldsymbol{k}')$ is the pairing interaction, which is essentially given by the low frequency limit of $\Gamma^{\rm pp}(k,k')$, $E_{\boldsymbol{k}}$ the Bogoliubov quasiparticle energy that is encoded in the Green function $G(\boldsymbol{k})$, and $\Delta(\boldsymbol{k})$ the superconducting energy gap. In fact, Eq. (45) is derived from a Bethe-Salpeter equation in the superconducting state analogous to the normal state equation (43) under a number of simplifying assumptions. Hence, we see that the leading eigenvector $\phi_{\rm lead}(K) \equiv \phi^R_{\rm lead}(K)$ is the normal state analog to the superconducting gap $\Delta(\boldsymbol{k})$. Close to the transition at $T = T_c$, they are equivalent.

3 Superconductivity in the 2D Hubbard model

We now demonstrate how the DMFT and DCA approaches have been used to investigate unconventional superconductivity in the simplest model of correlated electron systems, the 2D Hubbard model given by the Hamiltonian in Eq. (1) on a square lattice. We start by discussing the attractive model, which has $U < 0$, and then turn to the repulsive model with $U > 0$. While the former should be viewed as a toy model to study pairing, the latter has been studied extensively in the context of the high-T_c cuprates.

3.1 Attractive Hubbard model

The Hamiltonian of the attractive Hubbard model is given by the Hamiltonian in Eq. (1) with an attractive local Coulomb interaction $U < 0$. Since the Coulomb interaction between electrons is repulsive, i.e. positive, the negative U interaction should be considered an effective interaction that may result from integrating out other degrees of freedom, such as phonons in the case of the BCS model. In contrast to this case, however, the interaction U is an instantaneous static interaction without frequency dependence. Since the interaction between the electrons is explicitly attractive, this model provides an interesting toy model and testbed to study the superconducting phase transition as a function of the electron filling $\langle n \rangle$ and interaction strength $|U|/t$.

In fact, this problem has been studied extensively in the literature (see, e.g., Ref. [17] and references therein). As this model does not suffer from the usual fermionic negative sign problem, large scale quantum Monte Carlo simulations have been used to study the temperature versus $|U|$ phase diagram. One generally finds a finite temperature phase transition to a superconducting phase at finite doping $\langle n \rangle < 1$, while at half-filling $\langle n \rangle = 1$, this phase is suppressed to zero temperature by its degeneracy (due to particle-hole symmetry) with a charge-density wave (CDW) phase. As one moves away from half-filling, CDW correlations are suppressed and the superconducting T_c rises sharply. Since the pairing interaction U between electrons is local, one finds that the superconducting phase has s-wave symmetry, i.e., the Cooper pairs forming this state are local.

Because we are in 2D, for which the Mermin-Wagner theorem [18] forbids a finite temperature transition to a phase in which a continuous symmetry is broken, such as the U(1) gauge symmetry that is broken in the superconducting phase, the instability instead is a Kosterlitz-Thouless (KT) transition [19,20] to a superconducting state in which the correlations decay algebraically. DMFT and DCA calculations, however, do not obey the Mermin-Wagner theorem. They neglect the long range, beyond mean-field fluctuations that lead to the destruction of long-range order at finite temperature, the fundamental reason for this theorem. Due to their mean-field character, DMFT and DCA instead display mean-field type transitions. In DCA calculations, however, non-local fluctuations are taken into account up to the size of the cluster, and one may see KT behavior in a finite region above T_c, where the correlations are limited in range to within the cluster. Close to T_c, when the correlation length exceeds the cluster size, however, the KT behavior changes over to mean-field behavior.

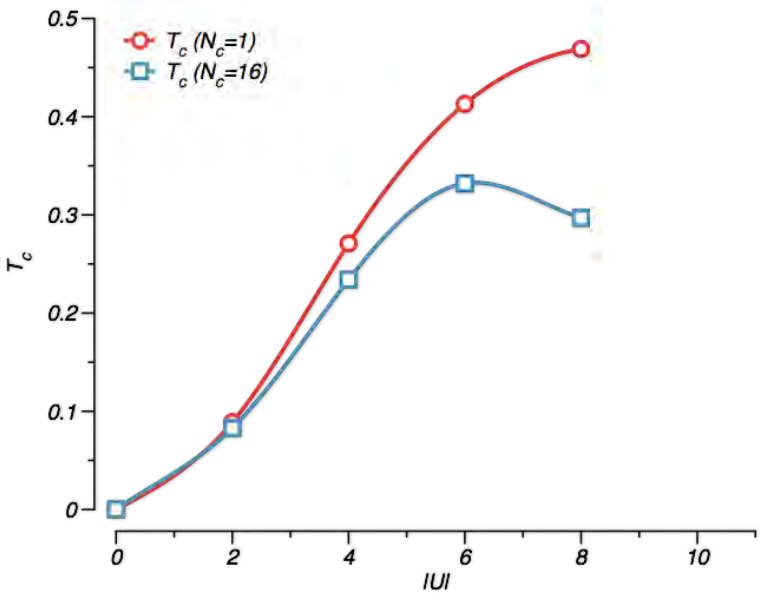

Fig. 6: Superconductivity in the attractive Hubbard model: *Transition temperature T_c in the negative U Hubbard model versus $|U|$ at a filling of $\langle n \rangle = 0.85$ calculated with DCA/QMC. T_c keeps rising with $|U|$ in the DMFT ($N_c = 1$) limit, while non-local fluctuations on the 4×4-cluster DCA calculation start suppressing T_c at larger $|U|$.*

Fig. 6 shows the results of single-site DMFT ($N_c = 1$) and 4×4-site DCA ($N_c = 16$) calculations of T_c in an attractive Hubbard model with nearest-neighbor hopping t and electron filling $\langle n \rangle = 0.85$. Here T_c for the s-wave superconducting state was determined from the temperature T at which leading eigenvalue $\lambda_s(T)$ of the Bethe-Salpeter equation (43) crosses one. We see that in both cases, T_c initially rises with increasing $|U|$. This is expected, since the increasing pair binding energy $\sim |U|$ leads to an increasing energy reduction associated with forming a superconducting phase, so that it occurs at higher temperatures.

At larger $|U|$, however, one observes different behavior: While T_c keeps rising for $N_c = 1$, it already starts to level off a bit. For $N_c = 16$, one even sees non-monotonic behavior, where T_c falls again after reaching a maximum for $|U| \sim 6t$. How can we understand this behavior, given the fact that with increasing $|U|$, the pair-binding energy keeps increasing? This behavior is known as the BCS-BEC crossover [21], where BEC stands for Bose-Einstein condensation. For small attractive interactions U, the physics is well described by BCS theory. The Cooper pairs are weakly bound and their size, determined by the superconducting coherence length $\sim 1/|U|$, is large. Therefore, the pairs have large spatial overlap, and as soon as they form, they become phase coherent. In contrast, in the large $|U|$ regime, the pairs are tightly bound and much more local objects. Hence, they have a harder time to become phase coherent, since the phase of individual pairs can fluctuate more easily. In this case, even though the pair-binding energy is large, T_c is suppressed, since phase coherence does not set in until lower temperatures are reached. DMFT only describes the spatially local aspect of this physics, i.e., phase fluctuations in time. Instead, the finite size clusters in the DCA also know about the spatial aspect of this physics, i.e., phase fluctuations of local pairs on different sites. This explains why T_c is reduced in the 16-site cluster relative to the single-site results.

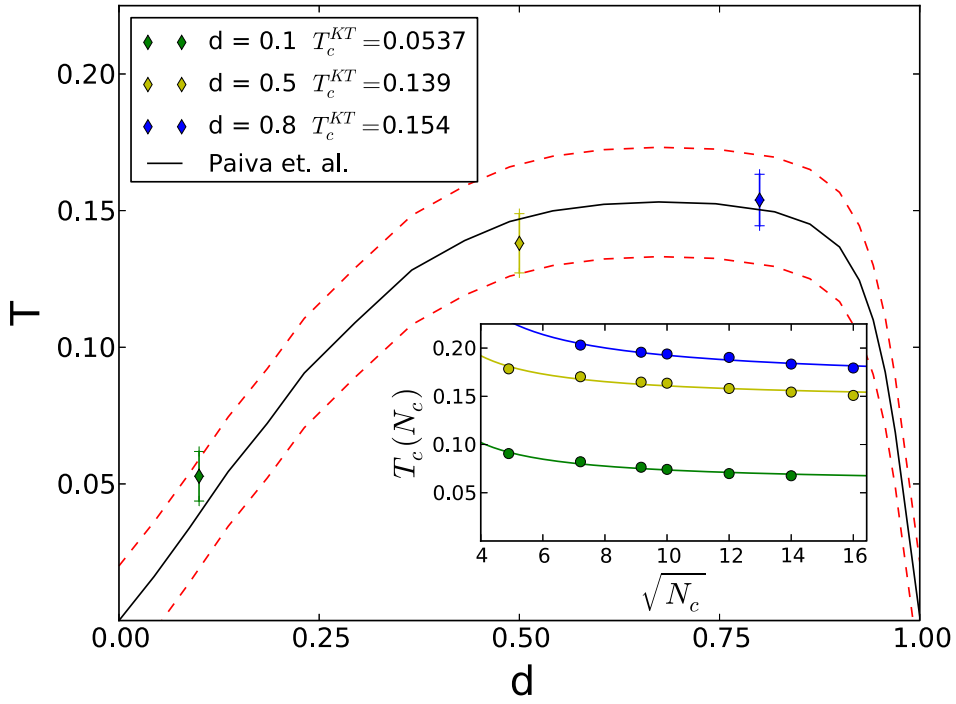

Fig. 7: Kosterlitz-Thouless transition temperature in the attractive Hubbard model: $T_c^{\rm KT}$ *for different electron densities* $d = \langle n \rangle$ *for* $U = -4t$ *calculated with DCA*$^+$*/QMC. The results were obtained by calculating* $T_c(N_c)$ *from the leading (s-wave) eigenvalue of the Bethe-Salpeter equation for different cluster sizes* N_c *and extrapolating the results to the exact* $N_c \to \infty$ *limit, where they compare well with finite size lattice DQMC calculations by Paiva et al. Figure from [22].*

In fact, for even larger clusters one would expect T_c to drop even more. An example of this is shown in Fig. 7, which displays the results of a DCA$^+$ calculation of T_c versus electron filling $d \equiv \langle n \rangle$ for $U = -4$. The inset shows the linear cluster size ($\sqrt{N_c}$) dependence of T_c for different $\langle n \rangle$, and one sees that T_c keeps dropping with increasing cluster size. For a filling of $\langle n \rangle = 0.8$, close to the filling used in Fig. 6, we see that $T_c \sim 0.25$ for $U = -4$ drops to ~ 0.15 in the infinite cluster size limit. Here, $T_c(N_c)$ was again determined from $\lambda_s(T_c(N_c)) = 1$ and the (exact) infinite cluster size limit $T_c(N_c \to \infty) \equiv T_{\rm KT}$ is obtained from fitting the $T_c(N_c)$ curves with the expected KT behavior [19, 20]

$$T_c(N_c) = T_{\rm KT} + \frac{A}{[B + \log(\sqrt{N_c})]^2} \,. \tag{46}$$

Here, we have assumed that the transition at finite N_c occurs at the temperature $T_c(N_c)$, at which the superconducting correlation length reaches the linear cluster size. The log arises from the fact that this correlation length has an exponential temperature dependence in the KT case.

The main panel in Fig. 7 shows T_c for different $\langle n \rangle$ determined this way. Also shown are results from finite size lattice determinant QMC calculations by Paiva *et al.* (solid black curve) [17]. We see that the DCA$^+$ results agree very well with those of Paiva *et al.*, showing that the DCA approximation and the procedures used to determine T_c provide reliable results.

3.2 Repulsive Hubbard model

We now turn to the 2D repulsive Hubbard model. Its Hamiltonian is given by Eq. (1) with $U > 0$. Unlike the attractive model, there is no explicitly attractive interaction in this model that could lead to superconductivity. Rather, the only interaction that is present is repulsive. Nevertheless, this model has been investigated extensively in the context of superconductivity, because it is commonly believed to provide a generic and the simplest description of the physics of cuprate high-temperature superconductors [9].

So how can a model with only a repulsive interaction have a superconducting instability? Various cluster DMFT and DCA studies have been concerned with addressing this question. Since the local Coulomb repulsion U in this model is large (a realistic description of the cuprates requires $U/t \gtrsim 6$), an s-wave superconducting state, in which the electrons are paired on the same site, is energetically unfavorable. Rather, one expects a state in which the electrons are paired on different sites. Since DMFT can only describe local order parameters, it is not adequate to study superconductivity in this model. Rather, one needs to use cluster extensions of DMFT, and here we focus on DCA studies of this problem.

Superconducting instability

If the Hubbard model is supposed to describe the cuprate high-temperature superconductors, then it should have a superconducting instability to a $d_{x^2-y^2}$-wave state with a $\cos k_x - \cos k_y$ momentum structure. By Fourier-transforming to real space, we see that in this state, the electrons are paired on nearest-neighbor sites with a $d_{x^2-y^2}$ phase (+1 along $\pm x$ and -1 along $\pm y$). Thus, one needs at least a 4-site 2×2 cluster to describe this state. The earliest DCA calculations of this problem were therefore done for a 2×2 cluster. The left panel in Fig. 8 shows the temperature versus doping $\delta = 1 - \langle n \rangle$ phase diagram of the 2D Hubbard model with $U/t = 8$ that resulted from this DCA $N_c = 4$ study [23]. And indeed, it has an extended $d_{x^2-y^2}$-wave superconducting phase at finite doping δ below the critical temperature T_c. Here T_c is the temperature T where the pair-field susceptibility in Eq. (41), $P_d(T)$, with a $d_{x^2-y^2}$-wave form factor $g_d(\boldsymbol{K}) = \cos K_x - \cos K_y$ diverges.

In addition, the phase diagram has an antiferromagnetic phase below the Néel temperature $T_{\rm N}$. This phase transition was determined in an analogous manner to that for the superconducting phase, by calculating the spin susceptibility $\chi_s(\boldsymbol{Q}, T) = \sum_{ij} e^{i\boldsymbol{Q}(\mathbf{x}_i - \mathbf{x}_j)} \int_0^\beta d\tau \, \langle \mathcal{T}_\tau S_i^z(\tau) S_j^z(0) \rangle$ for $\boldsymbol{Q} = (\pi, \pi)$, where $S_i^z = (c_{i\uparrow}^\dagger c_{i\uparrow} - c_{i\downarrow}^\dagger c_{i\downarrow})/2$ is the usual z-component of the spin operator. This is done in the same manner as for the pair-field susceptibility, i.e., within the framework described in Sec. 2.4, by calculating the irreducible vertex (in the spin $S = 1$ particle-hole channel) from the corresponding cluster susceptibility, and then using this vertex in the Bethe-Salpeter equation for the lattice susceptibility $\chi_s(\boldsymbol{Q}, T)$ [10]. Even though the Mermin-Wagner theorem (see discussion in Sec. 3.1) does not allow for an antiferromagnetic phase at finite T in the purely 2D model, the mean-field character of the DCA leads to this phase transition at finite T. In the real cuprate materials, it is the coupling between the copper-oxygen planes that stabilizes this transition at finite T.

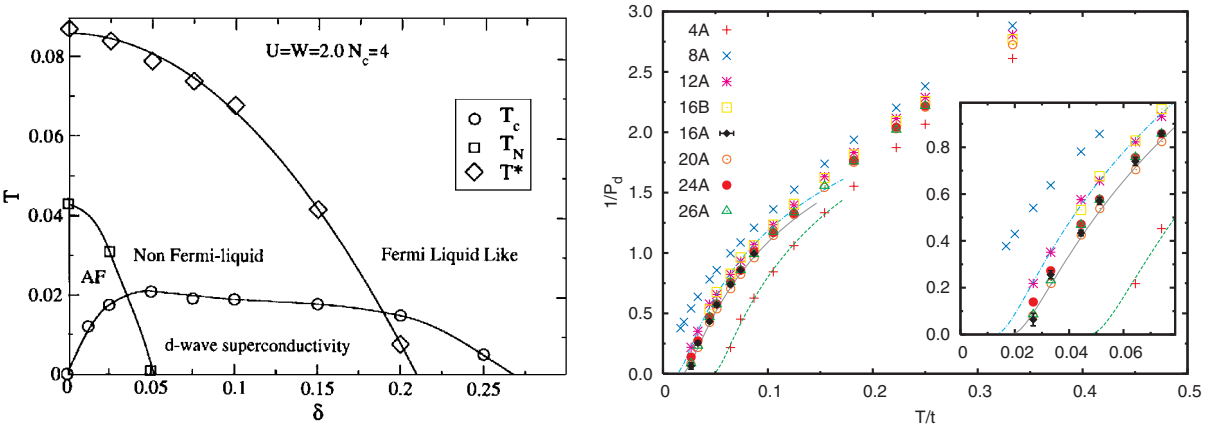

Fig. 8: D-wave superconductivity in the 2D repulsive Hubbard model: *Left panel: The temperature T versus doping $\delta = 1 - \langle n \rangle$ phase diagram calculated with DCA/QMC for a 2×2 cluster with $U = 8t$ has an antiferromagnetic phase near half-filling below $T_{\rm N}$, a d-wave superconducting phase at finite doping below T_c, and pseudogap behavior in the normal state below T^*. Right panel: Temperature dependence of the inverse pair-field susceptibility $1/P_d(T)$ calculated with DCA/QMC for different cluster sizes for $U = 4t$ and $\langle n \rangle = 0.9$. T_c is only weakly dependent on cluster size N_c when $N_c \gtrsim 12$. Figures from [23] (left) and [24] (right).*

The phase diagram also displays a line labeled T^*. This line does not indicate a phase transition. Rather, it indicates the temperature below which the bulk spin susceptibility $\chi_s(\boldsymbol{Q} = 0, T)$ starts to drop when the system is further cooled. This exotic behavior is very different from the Pauli susceptibility of a normal metal, which is basically independent of temperature at low T. The downturn in $\chi_s(\boldsymbol{Q} = 0, T)$ signals the opening of a pseudogap in the low energy spin excitations, which is also observed in various measurements in the cuprates [25]. In addition, at the same temperature T^*, the single-particle spectral function $A(\boldsymbol{k}, \omega) = -\mathrm{Im}\, G(\boldsymbol{k}, \omega + i\delta)/\pi$ starts to show a pseudogap, i.e., a partial suppression of spectral weight at the Fermi level $\omega = 0$. This is also observed in photoemission experiments in the cuprates, and provides evidence that not only the spin degree of freedom, but electronic excitations in general are suppressed at low energies. Thus, just like in the real materials, superconductivity in the Hubbard model emerges from an exotic state, which is very different from a normal metal.

Coming back to superconductivity, the question arises of what happens to the phase transition in more accurate calculations employing larger clusters when longer-ranged fluctuations are taken into account. Just like for the attractive Hubbard model, where the critical temperature is found to drop in larger clusters because of the inclusion of spatial phase fluctuations (see previous Sec. 3.1), we would expect T_c to fall when larger clusters are used. Does T_c go to zero or will it remain finite in the exact infinite size cluster limit? This question was first addressed with the larger cluster DCA calculations [24] of the pair-field susceptibility in a Hubbard model with $U = 4t$ and $\langle n \rangle = 0.9$ shown in the right panel of Fig. 8. Here, the temperature dependence of the inverse pair-field susceptibility $1/P_d(T)$ is plotted for a number of different cluster sizes and shapes (indicated by the letters 'A' and 'B' following the cluster size, see Ref. [24]), and the lines are fits to the exponential KT behavior one expects in two

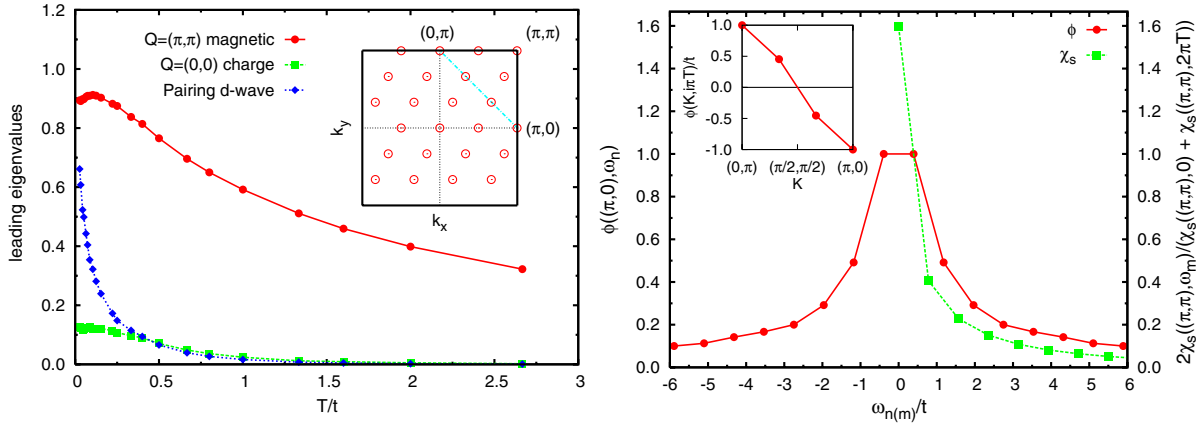

Fig. 9: Dominant correlations in the 2D repulsive Hubbard model: *DCA/QMC results for a 24-site cluster with $U = 4t$ and $\langle n \rangle = 0.85$. Left panel: Leading eigenvalues of the Bethe-Salpeter equation* (43) *in different channels. The $\boldsymbol{Q} = 0$ pairing eigenvalue has $d_{x^2-y^2}$-wave symmetry and increases towards one at low temperatures. The $\boldsymbol{Q} = (\pi, \pi)$ magnetic eigenvalue dominates but saturates at low temperatures, and the $\boldsymbol{Q} = 0$ charge eigenvalue remains small. The inset shows the position of the cluster momenta $\boldsymbol{K}$ in the 24-site cluster. Right panel: The frequency $\omega_n = (2n+1)\pi T$ dependence of the (normalized) leading $d_{x^2-y^2}$-wave pairing eigenvector $\phi_d(\boldsymbol{K}, \omega_n)$ for $T = 0.125t$ reflects the $\omega_m = 2m\pi T$ dependence of the (normalized) antiferromagnetic spin susceptibility $\chi_s(\boldsymbol{Q} = (\pi, \pi), \omega_m)$. The inset shows the $d_{x^2-y^2}$-wave $\cos K_x - \cos K_y$ momentum dependence of $\phi_d(\boldsymbol{K}, \omega_n = \pi T)$ along the dashed line shown in the left inset. Figure from [26].*

dimensions, i.e., $P_d(T) \sim \exp[2B/\sqrt{T - T_c}]$. We see that $1/P_d(T)$ goes to zero, i.e., $P_d(T)$ diverges, at a temperature $T_c(N_c)$ for most clusters, with the 4-site cluster clearly showing the largest $T_c \approx 0.05t$. As expected, for larger clusters T_c falls but is stabilized when $N_c \gtrsim 12$, for which $T_c \approx 0.02t$. More recent calculations [22] using the DCA$^+$ extension were able to go to even larger clusters, and found similar results with similar T_c in the large cluster limit. These calculations were also done for larger $U = 7t$, for which a larger $T_c \approx 0.05t$ was found. These calculations have thus provided evidence that the doped 2D Hubbard model has a d-wave superconducting instability at finite temperatures.

Pairing mechanism

So far, the calculations we have discussed are "numerical experiments", i.e., they show that a model, despite the presence of only repulsive interactions, can have a superconducting ground state, but do not give an answer to the question of what causes it. Unlike real experiments, however, we can directly analyze the effective interaction that gives rise to superconductivity in this model, i.e., the irreducible particle-particle vertex $\Gamma^{pp}(K, K')$ that enters the Bethe-Salpeter equation (43) for the pair-field susceptibility. This vertex describes the scattering of a pair of electrons with momenta and spins $(\boldsymbol{k} \uparrow, -\boldsymbol{k} \downarrow)$ to a pair of electrons with $(\boldsymbol{k}' \uparrow, -\boldsymbol{k}' \downarrow)$ (see Fig. 5). As discussed in Sec. 2.4, we can also study the leading eigenvalue and -vector of the Bethe-Salpeter equation and thus obtain new insight into this question.

The left panel of Fig. 9 shows the temperature dependence of the leading eigenvalue $\lambda_d(T)$ of the particle-particle Bethe-Salpeter equation (43) for $U = 4t$, $\langle n \rangle = 0.85$, calculated with DCA in the 24-site cluster shown in the inset [26]. As one sees from the blue curve, it rises sharply at low temperatures and approaches one, consistent with the divergence in the pair-field susceptibility. One can also construct similar Bethe-Salpeter equations for the charge and magnetic particle-hole channels. The leading eigenvalues for these channels are shown in red ($\boldsymbol{Q} = (\pi, \pi)$ magnetic) and green ($\boldsymbol{Q} = 0$ charge). We see that the magnetic eigenvalue is initially dominant, approaches one, but then saturates at values smaller than one at low temperatures. The leading eigenvalue in the charge channel, in contrast, remains small over the entire temperature range. From this, we can conclude that antiferromagnetic and superconducting correlations are the dominant correlations in the system.

The momentum dependence of the eigenvector $\phi_d(\boldsymbol{K}, \omega_n)$ corresponding to the leading pairing eigenvalue along the dashed line in the inset of the left panel is shown in the inset of the right panel. We see that it has a $d_{x^2-y^2}$-wave $\cos K_x - \cos K_y$ dependence. We note that in contrast to the calculation of the pair-field susceptibility, where a d-wave form factor is assumed, here this comes out naturally. The Matsubara frequency dependence of the pairing eigenfunction $\phi_d(\boldsymbol{K}, \omega_n)$ is shown in the main right panel and compared with the frequency dependence of the $\boldsymbol{Q} = (\pi, \pi)$ magnetic susceptibility $\chi_s(\boldsymbol{Q}, \omega_m)$. From this we see that (1) the pairing is retarded, i.e., frequency dependent, and (2) the pairing dynamics reflects that of the antiferromagnetic spin fluctuations.

We can also study the momentum and frequency dependence of $\Gamma^{\rm pp}(\boldsymbol{K}, \omega_n, \boldsymbol{K}', \omega_{n'})$ directly. Its momentum dependence is shown for three different temperatures in Fig. 10. We see that $\Gamma^{pp}(\boldsymbol{K}, \boldsymbol{K}')$ is peaked at large momentum transfer $\boldsymbol{K} - \boldsymbol{K}' = (\pi, \pi)$, and this peak increases in size as the temperature is lowered. This mirrors the growth of the antiferromagnetic spin fluctuations with decreasing temperature, as seen in the plot of $\chi_s(\boldsymbol{Q} = (\pi, \pi), \omega_m = 0)$ in the same figure.

Interestingly, we see that the pairing interaction $\Gamma^{\rm pp}$ in momentum space is positive, that is, repulsive! One may then ask: How does a repulsive interaction give rise to pairing? The answer lies in its momentum structure. If we look at the Bethe-Salpeter equation (43), or its simpler version, the BCS gap equation (45), we see that for an interaction $V(\boldsymbol{k}, \boldsymbol{k}') \equiv V$ that does not depend on momentum, a non-trivial solution $\Delta(\boldsymbol{k}) \neq 0$ only exists if $V < 0$. This follows from the minus sign on the left hand side and the fact that the other terms under the sum are all positive. This is the case for the conventional BCS superconductors or the attractive Hubbard model discussed in Sec. 3.1, for which $V < 0$ and the gap equation gives an s-wave gap $\Delta(\boldsymbol{k}) \equiv \Delta$ without momentum dependence.

In contrast, the pairing interaction we find for the Hubbard model is positive and has momentum dependence. In particular, it increases with increasing momentum transfer $\boldsymbol{k} - \boldsymbol{k}'$. The Fermi surface of the doped Hubbard model is schematically shown in the right panel of Fig. 11. It is similar to that of the hole-doped cuprates. The pairing interaction $V(\boldsymbol{k}, \boldsymbol{k}')$ scatters a pair with momenta $(\boldsymbol{k}, -\boldsymbol{k})$ to a pair with momenta $(\boldsymbol{k}', -\boldsymbol{k}')$ for $\boldsymbol{k}$ and $\boldsymbol{k}'$ near the Fermi surface and this scattering is strongest for a momentum transfer of $\boldsymbol{k} - \boldsymbol{k}' = (\pi, \pi)$. If the pairing gap $\Delta(\boldsymbol{k}')$

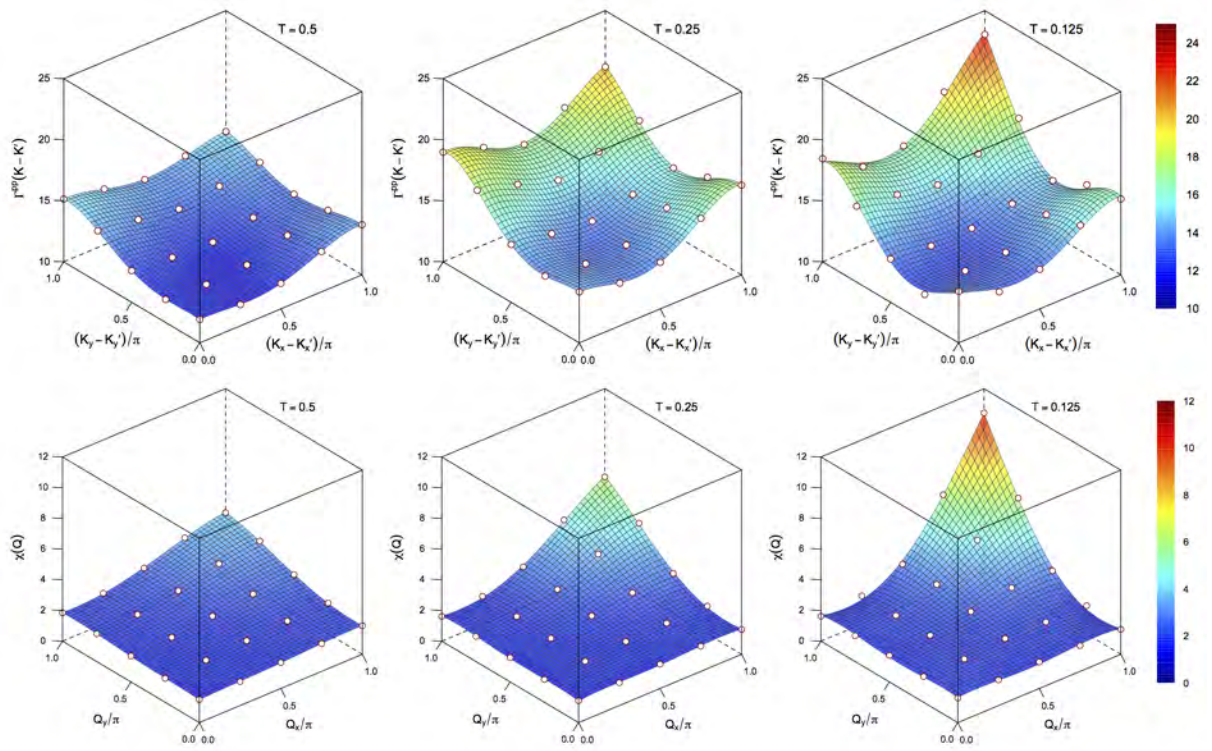

Fig. 10: Momentum structure of the pairing interaction in the 2D Hubbard model: *Top panel: $\boldsymbol{K}-\boldsymbol{K}'$ dependence of $\Gamma^{\rm pp}(\boldsymbol{K},\boldsymbol{K}')$ for $\omega_n=\omega_{n'}=\pi T$ calculated with DCA/QMC for a Hubbard model with $U=4t$ and $\langle n\rangle=0.85$ on a 4×4 cluster for different temperatures. Lower panel: $\boldsymbol{Q}$-dependence of the spin susceptibility $\chi_s(\boldsymbol{Q},\omega_m=0)$ for the same parameters. Both quantities display a similar increase near (π,π) as the temperature is lowered. Figure from [5].*

is positive for $\boldsymbol{k}'=(\pi,0)$, and $V(\boldsymbol{k}-\boldsymbol{k}')$ predominantly scatters pairs from $\boldsymbol{k}'=(\pi,0)$ to $\boldsymbol{k}=(0,\pi)$, the gap equation has a non-trivial ($\Delta(\boldsymbol{k})\neq 0$) solution if $\Delta(\boldsymbol{k})<0$ for $\boldsymbol{k}=(0,\pi)$. This is the case for a $d_{x^2-y^2}$-wave gap $\Delta(\boldsymbol{k})\sim cosk_x-\cos k_y$, which changes sign between $\boldsymbol{k}=(\pi,0)$ and $(0,\pi)$. Hence, the $d_{x^2-y^2}$-wave momentum structure of the gap arises naturally from a pairing interaction that is repulsive in momentum space and peaked at large momentum transfer. In fact a superconducting gap that changes sign on the Fermi surface generally signals a non-BCS like repulsive pairing interaction and therefore is taken as evidence for the presence of unconventional superconductivity [5].

How a repulsive pairing interaction that is peaked at (π,π) can lead to pairing can also be seen by Fourier-transforming the interaction $\Gamma^{\rm pp}(\boldsymbol{K},\boldsymbol{K}')$ to real space, according to

$$\Gamma^{\rm pp}(\ell_x,\ell_y)=\sum_{\boldsymbol{K},\boldsymbol{K}'} e^{i\boldsymbol{K}\ell}\,\Gamma^{\rm pp}(\boldsymbol{K},\boldsymbol{K}')\,e^{i\boldsymbol{K}'\ell}, \tag{47}$$

for $\omega_n=\omega_{n'}=\pi T$. Here, $\Gamma^{\rm pp}(\ell_x,\ell_y)$ is the strength of the $\omega_n=\omega_{n'}=\pi T$ pairing interaction between a singlet pair formed with one electron at the origin and the other at site (ℓ_x,ℓ_y). It is shown in the right panel of Fig. 11. We see that this interaction is strongly repulsive for on-site

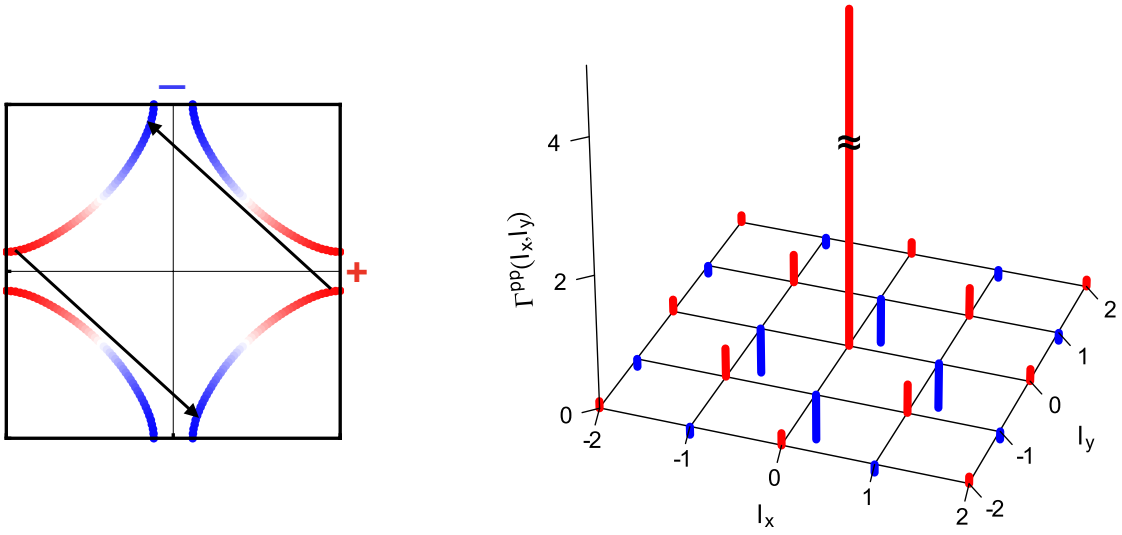

Fig. 11: D-wave pairing from repulsive interactions: *Left panel: Sketch of how repulsive scattering at large momentum transfer gives rise to $d_{x^2-y^2}$-wave pairing for the Fermi surface of a hole-doped Hubbard model. For this case, a gap that changes sign between the regions near $(\pi, 0)$ and $(0, \pi)$ satisfies the BCS gap equation* (45). *Right panel: Real space Fourier-transform $\Gamma^{\rm pp}(\ell_x, \ell_y)$, Eq.* (47)*, of the pairing interaction $\Gamma^{\rm pp}(\boldsymbol{K}, \boldsymbol{K}')$ for $\omega_n = \omega_{n'} = \pi T$ shown in Fig. 10 for $T = 0.125t$. Here red (blue) bars indicate positive (negative) values of $\Gamma^{\rm pp}(\ell_x, \ell_y)$ and the length of the bars corresponds to its magnitude. The pairing interaction is strongly repulsive for on-site pairs, but attractive when the electrons forming the pair sit on nearest-neighbor sites. Figure from [5].*

pairs, but attractive (negative) if the electrons are on nearest-neighbor sites. At longer distances, the interaction keeps oscillating but falls of rapidly with distance.

We have seen that the momentum and frequency structure of the pairing interaction given by the irreducible particle-particle vertex $\Gamma^{\rm pp}(\boldsymbol{k}, \omega_n, \boldsymbol{k}', \omega_{n'})$ reflects that of the spin fluctuations described by the spin susceptibility $\chi_s(\boldsymbol{q}, \omega_m)$. In fact, from weak coupling theory, one expects that

$$\Gamma^{\rm pp}(\boldsymbol{k}, \omega_n, \boldsymbol{k}', \omega_{n'}) \approx \frac{3}{2}\bar{U}^2 \chi_s(\boldsymbol{k} - \boldsymbol{k}', \omega_n - \omega_{n'}), \tag{48}$$

where $\bar{U}$ is a coupling constant. This form of the pairing interaction is only approximate, i.e., it only accounts for a subset of the Feynman diagrams that enter $\Gamma^{\rm pp}$. However, DCA studies have found that other contributions, such as the charge fluctuations, are negligible [16]. Hence, this approximate form has been shown to give a very good approximation of the "exact" DCA vertex $\Gamma^{\rm pp}$ and thus the resulting eigenvalues and -vectors of the Bethe-Salpeter equation, and therefore T_c [27]. One then speaks of a spin-fluctuation pairing interaction, in which the pairing is mediated by the exchange of (antiferromagnetic) spin fluctuations [5]. In contrast to the electron-phonon interaction, however, in this case the electrons that are being paired provide their own pairing glue, i.e., there are no separate degrees of freedom such as the phonons in conventional superconductors that mediate the pairing. Thus, it is not possible to separately tune the degrees of freedom that are being paired and the degrees of freedom that mediate the pairing. This makes it difficult to optimize T_c. One may see this by using a separable

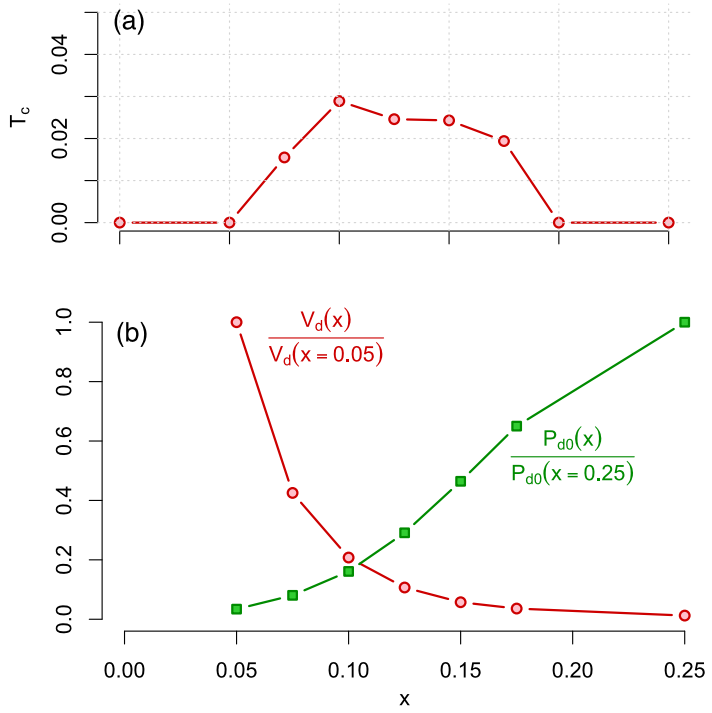

Fig. 12: Dome-shaped structure of the superconducting phase: *Top panel: Superconducting T_c versus doping x in the 2D Hubbard model with $U = 8t$ calculated with DCA/QMC for an 8-site cluster. Bottom panel: Normalized interaction strength V_d and intrinsic pair-field susceptibility $P_{d,0}$ versus doping x for $T = 0.125t$. The dome-like shape arises from competing trends in these two quantities as the doping varies. Figure from [28].*

approximation for $\Gamma^{\rm pp}$ [26],

$$\Gamma^{\rm pp}(K, K') \approx -V_d\, \phi_d(K)\, \phi_d(K'), \tag{49}$$

which becomes valid close to T_c when the d-wave eigenvalue λ_d is well separated from other eigenvalues. With this, the Bethe-Salpeter equation (43) for the d-wave eigenvalue becomes

$$V_d(T) P_{d,0}(T) \approx \lambda_d \tag{50}$$

with the "intrinsic" d-wave pair-field susceptibility $P_{d,0}(T) = T/N_c \sum_K \phi_d^2(K)\, \bar{G}^0_{2,\uparrow\downarrow}(K)$. The doping $x = 1 - \langle n \rangle$ dependence of $P_{d,0}(T)$ and $V_d(T)$ extracted from $V_d = \lambda_d / P_{d,0}$ via Eq. (50) is shown in the bottom panel of Fig. 12 together with the x-dependence of T_c. From this we see that the doping x, as a tuning parameter, has opposite effects on the strength of the pairing interaction V_d and the intrinsic pair-field susceptibility $P_{d,0}$, and thus T_c as seen in the top panel: With decreasing x, V_d rises, but $P_{d,0}$ falls, and the opposite behavior is observed with increasing x. The increase in V_d as half-filling ($x = 0$) is approached can be understood from the increase in the strength of the spin-fluctuations. The reason that this increase does not lead to an increase in T_c is that, at the same time, $P_{d,0}$ is suppressed. This can be understood from a reduction in the quasiparticle weight as the Mott state is approached. The interplay of the pairing strength V_d and the intrinsic pair-field susceptibility $P_{d,0}$ and their opposite doping dependence lead to the dome-shaped T_c seen in the top panel of Fig. 12.

3.3 Extended Hubbard model

In the conventional electron-phonon mechanism of superconductivity, retardation is a necessary ingredient in order to overcome the repulsive effect of the Coulomb interaction. In the Hubbard model, as well as in the cuprates, however, the d-wave structure of the Cooper pair wave function completely avoids the strongly repulsive effect of the local Coulomb U, because the electrons making up the pair sit on nearest-neighbor sites. Retardation is therefore not a necessary ingredient in this case. From the strong frequency dependence of the d-wave eigenvector shown in Fig. 9, however, we see that the pairing is nevertheless retarded on a scale set by the dynamics of the spin fluctuations.

The situation changes when an additional nearest-neighbor Coulomb repulsion

$$V \sum_{\langle ij \rangle, \sigma\sigma'} n_{i\sigma} n_{j\sigma'} \tag{51}$$

is considered and added to the Hubbard Hamiltonian in Eq. (1). The idea is that in realistic systems, the Coulomb repulsion is hardly screened to a purely local interaction, but has an additional short-ranged contribution. The resulting extended Hubbard model has recently been studied with DCA to examine the effect of V on d-wave superconductivity [29]. For d-wave pairs, where the electrons sit on neighboring sites, V is expected to have detrimental effects on superconductivity.

This is seen in the plot of T_c versus the strength of V shown in Fig. 13. These results were obtained from 2×2-cluster DCA calculations of the leading d-wave eigenvalue for the extended Hubbard model for $U = 7t$ and $\langle n \rangle = 0.9$. Although, as expected, T_c is reduced with increasing V, this decrease is rather modest, even up to relatively large values of V close to $U/2$. Why is d-wave superconductivity so robust with respect to a nearest-neighbor Coulomb repulsion V, which, in a static picture, will strongly reduce the binding energy of a d-wave pair and thus should rapidly suppress T_c? A clue lies in the frequency dependence of the pairing interaction.

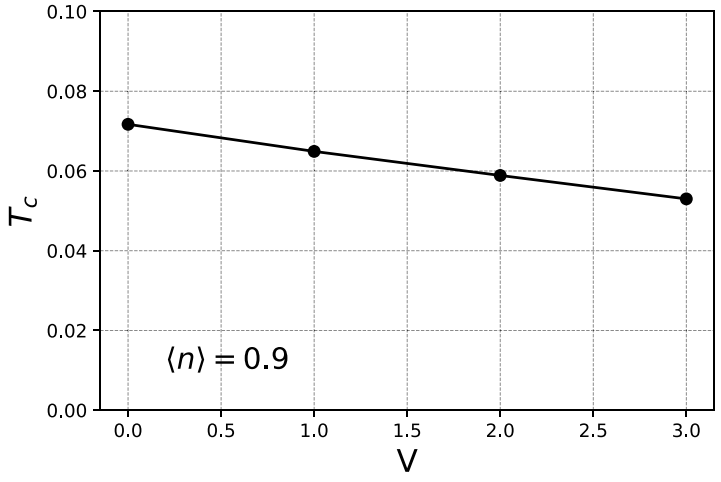

Fig. 13: Resilience of *d*-wave pairing to a nearest-neighbor Coulomb repulsion: *DCA/QMC 2×2-cluster results for T_c versus the nearest-neighbor Coulomb repulsion V in an extended 2D Hubbard model with $U = 7t$ and $\langle n \rangle = 0.9$. Figure from [29].*

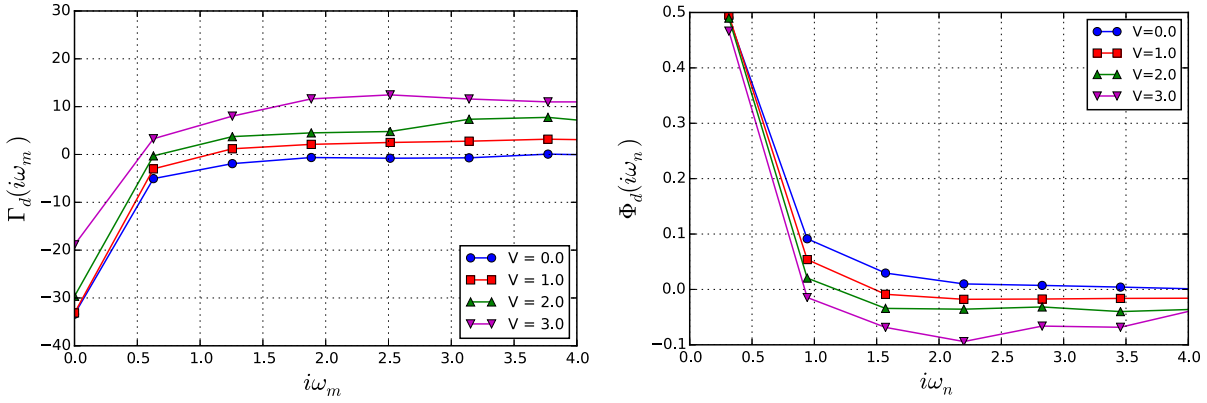

Fig. 14: The role of retardation in the pairing mechanism: *Left panel: DCA/QMC 2×2-cluster results for the d-wave projected pairing interaction $\Gamma_d(i\omega_m = i\omega_n - i\omega_{n'})$ with $\omega_{n'} = \pi T$ versus ω_m for different values of V for $\langle n \rangle = 0.9$ and $T = 0.1t$. Γ_d is attractive at low frequencies and for finite V turns repulsive at higher frequencies. Right panel: Frequency dependence of the leading d-wave eigenvector $\phi_d(\boldsymbol{K}, \omega_n)$ for $\boldsymbol{K} = (\pi, 0)$ for different values of V. The sign change in $\phi_d(\boldsymbol{K}, \omega_n)$ reduces the repulsive effect of V and thus stabilizes d-wave superconductivity. Figure from [29].*

Fig. 14 shows a plot of the d-wave projected pairing interaction

$$\Gamma_d(\omega_m = \omega_n - \omega_{n'}) = \frac{\sum_{\boldsymbol{K},\boldsymbol{K}'} g_d(\boldsymbol{K}) \Gamma^{\rm pp}(\boldsymbol{K}, \omega_n, \boldsymbol{K}', \omega_{n'}) g_d(\boldsymbol{K}')}{\sum_{\boldsymbol{K}} g_d^2(\boldsymbol{K})} \,. \tag{52}$$

Here $g_d(\boldsymbol{K}) = \cos K_x - \cos K_y$ and $\omega_{n'} = \pi T$. For $V = 0$, we see that $\Gamma_d(\omega_m)$ is negative over the whole frequency range. In other words, the pair scattering is attractive in the d-wave channel, as we know from the previous results for the standard model without V. When V is turned on, we see that $\Gamma_d(\omega_m)$ remains attractive at low frequencies, but then turns repulsive at higher frequencies. This reflects the fact that V is repulsive in the d-wave channel.

The dynamics of $\Gamma_d(\omega_m)$ is similar to that of the conventional electron-phonon superconductors, which is attractive at low frequencies due to the electron-phonon interaction, and repulsive at high frequencies due to the Coulomb repulsion. The effect of this sign change on the d-wave pairing eigenvector is shown in the right panel of Fig. 14, where the frequency dependence of $\phi_d(\boldsymbol{K}, \omega_n)$ is plotted for different values of V. As seen before in Fig. 9, for $V = 0$, it rapidly falls to zero. For finite V, however, we see that $\phi_d(\boldsymbol{K}, \omega_n)$ changes sign and turns negative at high frequencies, reflecting the sign change in the d-wave pairing interaction $\Gamma_d(i\omega_m)$. Thus, just as $\phi_d(\boldsymbol{K}, \omega_n)$ changes sign in $\boldsymbol{K}$ to adapt to the repulsive nature of the pairing interaction at large momentum transfer, $\phi_d(\boldsymbol{K}, \omega_n)$ also changes sign in frequency to adapt to the repulsive tail of the pairing interaction due to the Coulomb V. Therefore, just as in the electron-phonon case, retardation is important and necessary to protect the d-wave pairs from the repulsive effects of the (nearest-neighbor) Coulomb interaction.

4 Summary and concluding remarks

In these lecture notes, we have described how one can study superconductivity within the DMFT and DCA frameworks and how these approaches have been used to provide new insight into the nature of the pairing mechanism that leads to superconductivity in Hubbard models. As with other ordered states, there are always two alternative methods to determine a possible phase transition to a symmetry broken state within a mean-field approach like DMFT and DCA. The first option is to extend the algorithm to account for a finite order parameter that describes the symmetry broken state (anomalous propagator $\langle c_{\boldsymbol{k}\uparrow} c_{-\boldsymbol{k}\downarrow}\rangle$ in the case of superconductivity), and start the calculation with a finite field that couples to the order parameter. This field is then switched off after a few iterations and the calculation relaxes to either a state with order or without. One may also keep the field turned on during the full calculation, carry out calculations for different field strengths, and then calculate the response (susceptibility) to the field from the derivative of the order parameter with respect to the field. The transition temperature T_c is then obtained from the temperature where the susceptibility diverges. The second option is to carry out the usual normal state calculation in the absence of order or an external field, but instead calculate the susceptibility directly from the 4-point correlation function constructed from the order parameter. Since both DMFT and DCA approaches are thermodynamically consistent [7], both calculations will give identical results for the susceptibility and therefore T_c.

We have also seen that DMFT and DCA are powerful approaches to study superconductivity in Hubbard models. DMFT, due to its local nature, can only describe superconducting phases with order parameters that have a local contribution, such as s-wave. Applied to the attractive Hubbard model, it allows to study s-wave superconductivity, which is expected in the doped model due to its on-site attractive pairing potential $U < 0$. While it captures the rise of T_c with increasing $|U|$, DCA calculations employing larger clusters are needed to describe the downturn of T_c at large $|U|$ due to phase fluctuations.

For the repulsive Hubbard model, s-wave pairing is energetically unfavorable and therefore DMFT is not an adequate approach. DCA calculations employing a 2×2 cluster are the simplest possible calculations to study the $d_{x^2-y^2}$-wave pairing state that is expected for this model, which offers the most basic description of the cuprate high-temperature superconductors. And indeed, such 2×2-cluster DCA calculations have found properties reminiscent of the real materials, including antiferromagnetic, d-wave superconducting, and pseudogap behavior. DCA calculations also find that superconductivity remains stable in larger cluster calculations, providing evidence that the doped 2D Hubbard model does have a finite temperature d-wave superconducting transition.

Finally, we have seen that one can go beyond these numerical experiments and use these approaches to get insight into the mechanism that leads to pairing in these systems. Unlike real experiments, these calculations can be used to directly analyze the momentum and frequency structure of the pairing interaction. For the simple Hubbard model, one finds that it reflects the momentum structure of the spin fluctuations, and one speaks of a spin-fluctuation pairing interaction. Just as in the conventional electron-phonon case, this interaction is retarded on a scale

set by the dynamics of the antiferromagnetic spin fluctuations. While this retardation is not needed to overcome the local Coulomb repulsion in the simple Hubbard model, we have seen that it is essential in making the d-wave pairing state resilient to an additional nearest-neighbor Coulomb repulsion.

Because of the difficulty associated with solving the DMFT impurity or DCA cluster problem, most applications of these approaches in the field of superconductivity have been concerned with single-band Hubbard models. Additional orbital degrees of freedom must, however, be included in more complex models if one wants to study most materials other than the cuprates, such as, for example, the iron-based superconductors. While this remains a challenging but desirable task for the long term, more immediate progress may be made with simple toy models, such as the bilayer Hubbard model studied in Ref. [30], that have some overlap with the physics of the real materials.

Acknowledgments

I would like to acknowledge the close collaboration I have enjoyed with D.J. Scalapino and the many useful discussions and joint work with U. Hähner, M. Jarrell, M. Jiang, J. Keller, T. Pruschke, T.C. Schulthess and P. Staar. Support from the Center for Nanophase Materials Sciences is also acknowledged, which is a Department of Energy (DOE) Office of Science User Facility. Some of the material presented in these lecture notes was supported by the DOE Office of Science, Office of Advanced Scientific Computing Research, Scientific Discovery through Advanced Computing (SciDAC) program.

References

[1] J. Schrieffer: *Theory of Superconductivity* (Perseus Books, Reading, 1993)

[2] J. Bardeen, L.N. Cooper, and J.R. Schrieffer, Phys. Rev. **108**, 1175 (1957)

[3] A.B. Migdal, Sov. Phys. JETP **34**, 1438 (1958)

[4] G.M. Eliashberg, Soviet Physics JETP-USSR **11**, 696 (1960)

[5] D.J. Scalapino, Rev. Mod. Phys. **84**, 1383 (2012)

[6] A. Georges, W. Krauth, and M. Rozenberg, Rev. Mod. Phys. **68**, 13 (1996)

[7] T. Maier, M. Jarrell, T. Pruschke, and M. Hettler, Rev. Mod. Phys. **77**, 1027 (2005)

[8] J. Hubbard, Proc. Royal. Soc. London **276**, 238 (1963)

[9] P.W. Anderson, Science **235**, 1196 (1987)

[10] M. Jarrell, T. Maier, C. Huscroft, and S. Moukouri, Phys. Rev. B **64**, 195130 (2001)

[11] E. Gull, A.J. Millis, A.I. Lichtenstein, A.N. Rubtsov, M. Troyer, and P. Werner, Rev. Mod. Phys. **83**, 349 (2011)

[12] P. Staar, T. Maier, and T.C. Schulthess, Phys. Rev. B **88**, 115101 (2013)

[13] A. Lichtenstein and M. Katsnelson, Phys. Rev. B **62**, R9283 (2000)

[14] T. Maier, M. Jarrell, T. Pruschke, and J. Keller, Phys. Rev. Lett. **85**, 1524 (2000)

[15] T. Maier, M. Jarrell, T. Pruschke, and J. Keller, Eur. Phys. J. B **13**, 613 (2000)

[16] T.A. Maier, M.S. Jarrell, and D.J. Scalapino, Phys. Rev. Lett. **96**, 047005 (2006)

[17] T. Paiva, R.R. dos Santos, R. Scalettar, and P. Denteneer, Phys. Rev. B **69**, 184501 (2004)

[18] N. Mermin and H. Wagner, Phys. Rev. Lett. **17**, 1133 (1966)

[19] J. Kosterlitz, J. Phys. C **7**, 1046 (1973)

[20] J. Kosterlitz and D. Thouless, J. Phys. C **6**, 1181 (1973)

[21] Q. Chen, J. Stajic, S. Tan, and K. Levin, Phys. Rep. **412**, 1 (2005)

[22] P. Staar, T. Maier, and T.C. Schulthess, Phys. Rev. B **89**, 195133 (2014)

[23] M. Jarrell, T. Maier, M.H. Hettler, and A. Tahvildarzadeh, Europhys. Lett. **56**, 563 (2001)

[24] T.A. Maier, M. Jarrell, T.C. Schulthess, P.R.C. Kent, and J.B. White, Phys. Rev. Lett. **95**, 237001 (2005)

[25] M.R. Norman, D. Pines, and C. Kallin, Adv. Phys. **54**, 715 (2005)

[26] T.A. Maier, M. Jarrell, and D. Scalapino, Phys. Rev. B **74**, 094513 (2006)

[27] T.A. Maier, A. Macridin, M. Jarrell, and D.J. Scalapino, Phys. Rev. B **76**, 144516 (2007)

[28] T.A. Maier, J. Supercond. Nov. Magn. **25**, 1307 (2012)

[29] M. Jiang, U.R. Hähner, T.C. Schulthess, and T.A. Maier, Phys. Rev. B **97**, 184507 (2018)

[30] T. Maier and D. Scalapino, Phys. Rev. B **84**, 180513(R) (2011)